Title: Exploiting Molecular Symmetry to Quantitatively Map the Excited-State Landscape of Iron-Sulfur Clusters

Authors: Brighton A. Skeel and Daniel L.M. Suess*

Address: Department of Chemistry, Massachusetts Institute of Technology, Cambridge, Massachusetts 02139, United States.

Contact information: suess@mit.edu

Abstract

Cuboidal [Fe_4S_4] clusters are ubiquitous cofactors in biological redox chemistry. In the $[Fe_4S_4]^{1+}$ state, pairwise spin coupling gives rise to six arrangements of the Fe valences ('valence isomers') amongst the four Fe centers. How a protein active site dictates the arrangement of the valences in the ground state, as well as the population of excited-state valence isomers, is poorly understood in part because of the magnetic complexity of these systems. Here, we show that the ground-state valence isomer landscape can be simplified from a six-level system in an asymmetric protein environment to a two-level system by studying the problem in synthetic clusters $[Fe_4S_4]^{1+}$ clusters with solution C_{3v} symmetry. This simplification allows for the small energy differences between valence isomers (sometimes < 0.1 kcal/mol) to be quantified by simultaneously fitting the VT NMR and solution magnetic moment data. Using this fitting protocol, we map the excited state landscape for a range of clusters of the form $[(SIMes)_3Fe_4S_4–X/L]^n$, (SIMes = 1,3-dimesityl-imidazol-4,5-dihydro-2-ylidene; $n = 0$ for anionic, X-type ligands, and $n = +1$ for neutral, L-type ligands) and find that a single ligand substitution can alter the relative energies of valence isomers by at least 10^3 cm^{-1}. On this basis, we suggest that one result of 'non-canonical' amino acid ligation in Fe–S proteins is to alter the distribution of the valence electrons in the manifold of thermally populated excited states.

Main text

Introduction

Biological Fe–S clusters perform a range of critical cellular functions, including serving as conduits for electron transfer and catalyzing kinetically challenging reactions.[1,2] As for any metallocofactor, the protein environment plays an important role in dictating the cluster's electronic structure, properties, and reactivity. For metalloclusters, which can feature substantial and highly variable degrees of electron delocalization, these effects must be understood not just in the context of the cluster as a whole (*e.g.*, its redox properties),[3–14] but also in terms of its individual metal ions (*e.g.*, at which site(s) redox chemistry takes place).[15,16] In this paper, we study the electron distribution in synthetic models of Fe–S cofactors with the goals of (i) learning which Fe sites are oxidized/reduced in the ground state, (ii) quantifying the energies of excited states featuring alternative valence arrangements, and (iii) understanding to what extent the favorability of these valence arrangements is controlled by the cluster's primary coordination sphere.

Germane to this topic is the nature of electron delocalization in Fe–S clusters. Whereas the smallest cluster structures typically exhibit valence trapping (*i.e.*, the discrete Fe^{2+} and Fe^{3+} ions in $[Fe_2S_2]$ clusters, with a few exceptions showing varying degrees of delocalization[16–20]), larger clusters usually have more delocalized electronic structures. We focus here on the most ubiquitous Fe–S cluster structure type, the cuboidal $[Fe_4S_4]$ clusters (and specifically the $[Fe_4S_4]^{1+}$ state), whose electronic structures have historically been discussed using the Heisenberg-Dirac-van Vleck (HDvV) model,[21] and more contemporarily using the Heisenberg double exchange (HDE) model. Under certain simplifying assumptions, each may be solved analytically for $[Fe_4S_4]^{n+}$ clusters.[22,23] The electronic structures of these clusters have additionally been scrutinized with greater levels of detail including (but not limited to) vibronic coupling models, broken-symmetry density functional theory (BS-DFT), and wavefunction-based computational methodologies.[24–30] Two hallmarks of the electronic structure picture for $[Fe_4S_4]$

clusters that emerge at all modern levels of theory are that (i) antiferromagnetic coupling is maximized by having two Fe centers with majority spin and two with minority spin, and (ii) for mixed-valent clusters, Fe^{3+} and Fe^{2+} ions undergo spin-dependent electron delocalization (double exchange) to give pairs of $Fe^{2.5+}$ centers.[23] For the ground states of $[Fe_4S_4]^{1+}$ clusters, this is manifested as a pair of $2\times Fe^{2.5+}$ ions (with net majority spin) antiferromagnetically coupled to two Fe^{2+} ions, each with net minority spin; similar pairwise coupling schemes describe the electronic structures of the $[Fe_4S_4]^{2+}$ and $[Fe_4S_4]^{3+}$ states.[31] Thus, the 'extra' electron in $[Fe_4S_4]^{1+}$ clusters (or, alternatively, the 'hole' in $[Fe_4S_4]^{3+}$ clusters) relative to the $[Fe_4S_4]^{2+}$ state is neither fully delocalized nor localized at a single Fe site, and instead resides on a pair of Fe ions.

One consequence of this partial delocalization is that the various arrangements of Fe valences are energetically inequivalent, a phenomenon known as 'valence isomerism' (also referred to as electromerism, valence tautomerism, or redox isomerism), where a specific valence isomer is defined by its unique arrangement of valences (see Figure 1A for valence isomerism in $[Fe_4S_4]^{1+}$ clusters). Valence isomerism has been studied both theoretically and experimentally in some transition-metal-containing[32–38] and organic systems[39,40] as well as in Fe–S clusters, where it was first suggested as an explanation for the unusual variable-temperature (VT) ^{1}H NMR behavior of the cysteine thiolates coordinated to the $[Fe_4S_4]^{3+}$ cluster in some high potential iron proteins (HiPIPs).[41] Since this original proposal, valence isomerism has been studied more broadly, including in additional HiPIPs,[8,42–44] in reduced ferredoxins (in the $[Fe_4S_4]^{1+}$ state),[45] in computational work on reduced $[Fe_4S_4]^{1+}$ clusters,[46] and in $[Fe_2S_2]^{+}$ clusters.[16] The sustained interest in valence isomerism in Fe–S clusters stems in part from its potential functional relevance; indeed, rates of electron transfer from Fe–S proteins in many cases have dependencies on both relative cluster-accepter orientation[47] and the ligands binding the cluster,[48–50] the latter consideration dictating in part the valence isomer distribution for the cluster. Valence rearrangements (coupled to the accompanying spin rearrangements) have also been proposed to be functionally relevant in catalysis by

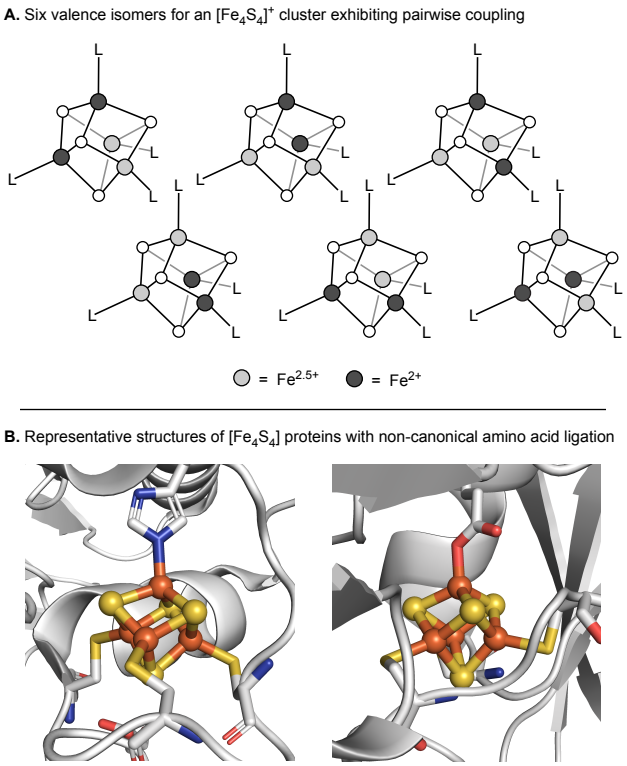

Figure 1. Valence isomerism in $[Fe_4S_4]^{1+}$ clusters. A) For pairwise coupling schemes, there are six valence isomers in $[Fe_4S_4]^{1+}$ clusters. B) Examples of 3:1 site-differentiated $[Fe_4S_4]$ clusters in biology. Images generated from PDB 3C8Y (*C. pasteurianeum* [FeFe]-hydrogenase, left) and 3NOY (*E. coli* IspG, right).

radical *S*-adenosylmethionine (SAM) enzymes[51,52] and electron transfer in biological nitrogen fixation.[53] In regards to the main focus of this paper—understanding the importance of the primary coordination sphere on affecting valence isomerism in $[Fe_4S_4]^{1+}$ clusters—we highlight seminal work on the *Pyrococcus furiosis* ferredoxin (*Pf* Fd) and mutants thereof that demonstrated that single point mutations can shift the positions of the spin-aligned pairs of Fe sites.[54–56] Further interest in the role of the primary coordination sphere in altering the distribution of electrons has been fueled by the discovery of additional examples of $[Fe_4S_4]^{1+}$ clusters in biology featuring 'non-canonical' (*i.e.*, non-cysteinyl) amino acid ligation (examples of which are shown in Figure 1B).[49,57–61]

Despite the importance of understanding valence isomerism, as well as many groundbreaking studies of this phenomenon in Fe–S proteins (mentioned above and further discussed throughout), the inherent asymmetry of the protein environment makes *quantifying* the energy difference between valence isomers exceedingly difficult. First, the pairwise coupling scheme in $[Fe_4S_4]^{1+}$ clusters results in six valence isomers (Figure 1A), and because each Fe site in a biological cluster is electronically unique (even when part of a homoleptic primary coordination sphere (e.g., Cys_4)), each valence isomer is energetically inequivalent. As such, obtaining a quantitative picture of valence isomerism requires characterizing five energy differences between the ground states of each valence isomer. Second, each valence isomer is also magnetically unique, and therefore six spin ladders must be modeled when analyzing data acquired at non-cryogenic temperatures (*e.g.*, in solution NMR experiments), resulting in an intractably large parameter space. Moreover, if a systematic understanding of how a cluster's primary coordination sphere impacts the valence isomer landscape is to be developed, one prerequisite is that primary-sphere effects must be studied in isolation from others (*e.g.*, secondary-sphere effects), which is challenging to achieve in relatively ordered polypeptides because mutation of a coordinating amino acid residue can have longer-range effects (*e.g.*, resulting in changes in H-bonding networks, rearrangements of the active site, etc.). Because it is difficult to decouple these effects from one another, it is not always clear to what extent 'non-canonical' amino acid ligation alone (*i.e.*, in the absence of other effects beyond the primary coordination sphere) alters the energetic landscape of valence isomers.

Given these considerations, we sought a system that would both have a simpler electronic landscape and allow for precise control over the primary coordination sphere, and we herein report a family of $[Fe_4S_4]^{1+}$ clusters that has the requisite solution symmetry and synthetic tunability for these purposes. Specifically, their 3:1 symmetry simplifies the ground-state valence isomer landscape to a two-level system, allowing for the energy difference to be determined through simultaneous fitting of their VT NMR spectra and magnetic moments. In applying this analysis to a diverse array of 3:1 site-differentiated

clusters, we experimentally delineate several factors that govern the valence electron distributions of Fe–S clusters and quantitatively assess the extent to which a single substitution in the primary sphere can alter the excited state landscape, with particular attention paid to ligands of biological relevance.

The Results section is organized as follows: (1) a brief survey of how paramagnetic NMR spectroscopy can provide insights into the distribution of spin in $[Fe_4S_4]^{1+}$ clusters, including a discussion of the influence of symmetry on the valence isomer landscape; (2) an overview of our approach to modeling the VT NMR and magnetic moment properties to extract information about each cluster's magnetic structure; (3) the synthesis and characterization of the clusters; (4) a qualitative description of the clusters' NMR properties; (5) quantitative NMR analysis of a representative example; (6) comparative analysis of all clusters' valence isomer landscapes; (7) discussion of the temperature dependence of the valence electron distribution.

Materials and Methods

Synthetic methods

Unless noted, all synthetic procedures and manipulations were carried out using standard Schlenk techniques under an atmosphere of dry N_2 or in an LC Technologies glovebox under an atmosphere of N_2 (< 1 ppm O_2/H_2O). Detailed synthetic procedures can be found in the SI.

VT NMR Sample Preparation, Data Acquisition, Fitting, and Error Analysis

In a typical run, 8-12 mg of the appropriate complex was weighed into a glass scintillation vial. To this vial was added a volume of the chosen NMR solvent sufficient to fully dissolve the sample, followed by additional solvent (to prevent low-temperature precipitation). The mass of this solvent was recorded for later volume calculations. A portion of this solution was transferred to a J. Young style NMR tube containing a flame sealed glass capillary filled with the same dry and deoxygenated NMR solvent. The sample was then sealed and analyzed immediately. Following data collection, samples were re-analyzed at room temperature with identical acquisition parameters to verify that no decomposition or precipitation had occurred. These spectra were then analyzed in MestReNova (version 14.2.1-27684). Spectra were referenced to the lowest-frequency residual solvent peak of the sample capillary, phased manually, and baseline-corrected using a manual multipoint method with cubic spline interpolation between points. Peak positions were extracted by fitting peaks to Lorentzian/Gaussian lineshapes. Solution magnetic moments were computed using the method of Evans[62] and have been corrected for diamagnetic contributions using Pascals constants.[63] Solution densities were corrected for the effects of deuteration by multiplying the density of the fully protonated solvent with the molecular weight ratio between the perdeutero and proteo solvents (*i.e.*, by assuming deuteration does not appreciably effect molecular volume). Solvent densities were further corrected for density changes as a function of temperature.[64]

Fits to these data were generated in MATLAB using the lsqcurvefit functionality by minimizing the value of the target function corresponding to the residuals between computed and observed NMR chemical shifts as well as magnetic moments (code and additional details provided in the SI). Twenty fit families for each complex were generated, each by randomly altering the assumed diamagnetic shift value, assuming a normal distribution with 0.1 ppm variance about an assumed diamagnetic shift, corresponding to the protonated ligand (for X-type ligands), or the free ligand (for L-type ligands) in C_6D_6 at ambient temperature. For **1-SePh** and **1-TePh**, the chemical shifts of $(PhSe)_2$ and $(PhTe)_2$ were used.

Fits with errors greater than three standard deviations larger than the mean were rejected, and the remaining fits were averaged to give the final reported parameters. Individual fits were produced by sampling a wide range of initial conditions using MATLAB's manymins functionality so as to avoid identifying a local but not global fit minimum. The number of initial conditions required to satisfactorily identify a global minimum was determined as described in the error estimation section of the SI. The numeric weighting scheme for this nonlinear least squares routine is such that magnetic moments (input as Bohr magnetons) are multiplied by a factor of 10, and the paramagnetic parts of the chemical shift are scaled by a factor of $(\Delta\delta)^{-1/2}$ where $\Delta\delta$ is the maximum change of a given resonance over the measured temperature range, in ppm. Numerically, this scaling brings all values into gamut with one another, and prevents one observation alone from dominating the fit. A representative fitting routine is provided in the SI.

Results

1. NMR Properties of Fe–S Clusters

We first summarize relevant aspects of paramagnetic NMR analysis for Fe–S clusters, most of which have been previously described in studies of Fe–S proteins, and many of which feature prominently in the history of paramagnetic NMR analysis generally.[6,41,66–75] For any nucleus in a paramagnetic molecule, the paramagnetic component (δ_{para}) of the observed chemical shift (δ_{obs}) is given by

$$\delta_{para} = \delta_{obs} - \delta_{dia} \quad \text{(EQ. 1)}$$

where δ_{dia} is the component of the chemical shift arising from diamagnetic contributions. δ_{para} may be further decomposed into contributions arising from either contact (through-bond, δ_{con}) or pseudocontact (through-space, δ_{pcs}) terms as follows:

$$\delta_{para} = \delta_{con} + \delta_{pcs} \quad \text{(EQ. 2)}$$

The latter term depends on the extent of spin-orbit coupling (manifested as *g*-anisotropy) present in a system and, for the specific case of Fe−S clusters, is a minor contributor relative to the contact shift component of δ_{para}.[69] As such, we consider only contributions from δ_{con} in our analyses. This term takes the following form for molecular systems with one open-shell center where the Curie law is obeyed and spin-orbit effects are negligible:[76]

$$\boldsymbol{\delta_{con}} = \frac{\boldsymbol{A}}{\hbar}\frac{\boldsymbol{g_e \mu_B S(S+1)}}{\boldsymbol{3\gamma_I k_B T}} \quad \text{(EQ. 3)}$$

where A is the electron-nuclear hyperfine coupling, g_e is the free electron g-value, μ_B is the Bohr magneton, S is the total electron spin quantum number, γ_I is the gyromagnetic ratio of the nucleus of interest, k_B is the Boltzmann constant, and T is the absolute temperature.

The same physical principles apply to the NMR spectra of Fe–S clusters, with the additional caveats that at room temperature many excited spin states are populated and that the orientations of Fe-centered spins relative to the total cluster spin moment within these states are beholden to the exchange coupling interactions between Fe sites. For odd-electron, cuboidal [Fe_4S_4] clusters, these exchange interactions are typically described using the "pair-of-pairs" Hamiltonian, which affords maximal antiferromagnetic coupling for $J > 0$ cm^{-1}:

$$\hat{H} = J \sum_{1 \le m < n \le 4} \vec{S}_m \cdot \vec{S}_n \pm B\left(S_{34} + \frac{1}{2}\right) + \Delta J_{12}\left(\vec{S}_1 \cdot \vec{S}_2\right) + \Delta J_{34}\left(\vec{S}_3 \cdot \vec{S}_4\right)$$

(EQ. 4)

Here, $\vec{S}_m$ and $\vec{S}_n$ denote the site spins of metal centers m and n respectively. For an [Fe_4S_4] cluster, we number the Fe centers 1-4, the relevant pairs then being the Fe1-Fe2 pair and the Fe3-Fe4 pair. The parameter J is the base exchange coupling constant between Fe centers m and n, and the values ΔJ_{12} and ΔJ_{34} are the differences in exchange coupling constant within the Fe1-Fe2 and Fe3-Fe4 pairs relative to J (*i.e.*, the coupling between Fe1 and Fe2 is $J + \Delta J_{12}$, and that between Fe3 and Fe4 is $J + \Delta J_{34}$). We take the convention that the Fe3-Fe4 pair is the mixed-valence pair with associated double exchange parameter B, which is introduced to this Hamiltonian in a phenomenological manner. Despite some limitations (*e.g.*, in capturing the density of excited states),[27,29] this Hamiltonian has successfully explained many aspects of the electronic structures of Fe–S clusters, including their variable-temperature magnetic behaviors, their ground spin states, and their ^{57}Fe hyperfine coupling values.[21,22,77–80]

For a cuboidal [Fe_4S_4] cluster, the chemical shifts of $I \neq 0$ nuclides that experience paramagnetic contact shifts due to the cluster's spin moment are given by:[81]

$$\delta_{para} = \frac{g_e \mu_B}{\hbar \gamma_I 3 k_B T} A_m \frac{\Sigma_i C_{im} S_i (S_i + 1)(2S_i + 1) e^{-E_i/k_B T}}{\Sigma_i (2S_i + 1) e^{-E_i/k_B T}}$$

(EQ. 5)

Here, A_m is a fictitious electron-nucleus hyperfine coupling constant between the nucleus of interest and a particular metal site *m* within the cluster in the absence of any magnetic exchange interactions. This value is not the same as the observed hyperfine coupling in the magnetically coupled system (*i.e.*, what one would obtain in an EPR experiment). The value C_{im} is a spin projection coefficient that describes the projection of metal site *m*'s spin onto the total spin of a given state *i* (the eigenstates of the Hamiltonian in Eq. 4, and the value E_i is the energy of the state *i*. The summations appearing in the numerator and denominator reflect that the observed paramagnetic shift is the expectation value for the canonical ensemble description of all populated states, with the $2S_i + 1$ term accounting for differences in spin-state multiplicity between spin eigenstates. By describing δ_{para} in this way, it is implied that interconversion between excited states is rapid relative to the NMR timescale and that one resonance per magnetically unique nuclide is observable; to the best of our knowledge, this is the case for every known [Fe_4S_4] cluster.

For systems with an odd number of electrons ([Fe_4S_4]$^{1+/3+}$ clusters), the additional considerations of valence isomerism and, consequently, molecular symmetry, become relevant. In particular, we must sum over not only the sets of thermally populated states associated with one spin system (corresponding to one valence localization pattern), but over all thermally populated states associated with each spin ladder for every possible valence localization pattern—of which there are six within the pair-of-pairs framework—taking into account that the energy of the lowest rung of the spin ladder may differ for each valence isomer.

In more detail, the energies and degeneracies of the six valence isomers ligands in a generic $[Fe_4S_4]^{1+}$ cluster are dictated by its ligands. For a homoleptic cluster in solution, each valence isomer is chemically equivalent and therefore isoenergetic (Figure 2A). For a 3:1 site differentiated cluster (*i.e.*, a cluster of the form $[Fe_4S_4(L)_3(L')]$, where $L \neq L'$), there are two families of three triply degenerate valence isomer states (Figure 2). For an $[Fe_4S_4]^{1+}$ cluster, these valence isomer families are characterized by the presence of either $Fe^{2.5+}$ at the unique site (valence isomer A, VI_A) or Fe^{2+} at the unique site (valence isomer B, VI_B). These two valence isomers are in turn related to one another by the difference in their ground-state energies; we refer to this difference for a cluster of any symmetry as an offset energy, and as ΔE_{VI} for the 3:1 differentiated clusters studied herein. By convention, we take ΔE_{VI} as the energy by which VI_A is stabilized over VI_B:

$$\Delta E_{\mathrm{VI}} = E(\mathrm{VI_B}) - E(\mathrm{VI_A})$$

(EQ. 6)

The other possible symmetries for the ligand sphere of a tetrahedral cluster with pairwise electronic coupling are 2:2, 2:1:1, and 1:1:1:1 differentiation (the latter being a fully heteroleptic cluster, as is found in a protein environment, for example), each with two, three, and five offset energies, respectively. Thus, among heteroleptic clusters, the 3:1 site-differentiation pattern affords the simplest landscape of valence isomers, and as described below, this feature simplifies spectroscopic analysis and makes quantitative determinations of ΔE_{VI} feasible.

We now consider how symmetry impacts the observed VT NMR behavior of clusters subject to valence isomerism. Each equivalent ligand bound to an $[Fe_4S_4]^{1+}$ cluster introduces a simplifying element to the valence isomer landscape. For homoleptic clusters, the equilibrium geometries of each valence isomer in solution are identical and isoenergetic. Thus, on the NMR timescale, each Fe center has equal portions Fe^{2+} and $Fe^{2.5+}$ character, and correspondingly each chemically equivalent ligand nucleus has the same chemical shift despite the ground state electronic symmetry of the cluster being maximally C_{2v} (Figure 2B). In the ground state, the pair of mixed-valence Fe ions is maximally $S = 9/2$ and aligns with the applied field, whereas the pair of ferrous Fe ions is maximally $S = 4$, aligned anti-parallel with respect to the applied field[82]—these valence-dependent spin patterns are additionally true for most excited states produced by this vector coupling model. Ligand nuclides in homoleptic $[Fe_4S_4]^{1+}$ clusters then tend to experience both positive and negative contributions to their contact shifts of competing magnitudes, and as a result, have nearly temperature-independent VT NMR behavior. This partial 'cancelation' of the contributions to the contact shift is diminished in heteroleptic clusters for which the ground-state energies

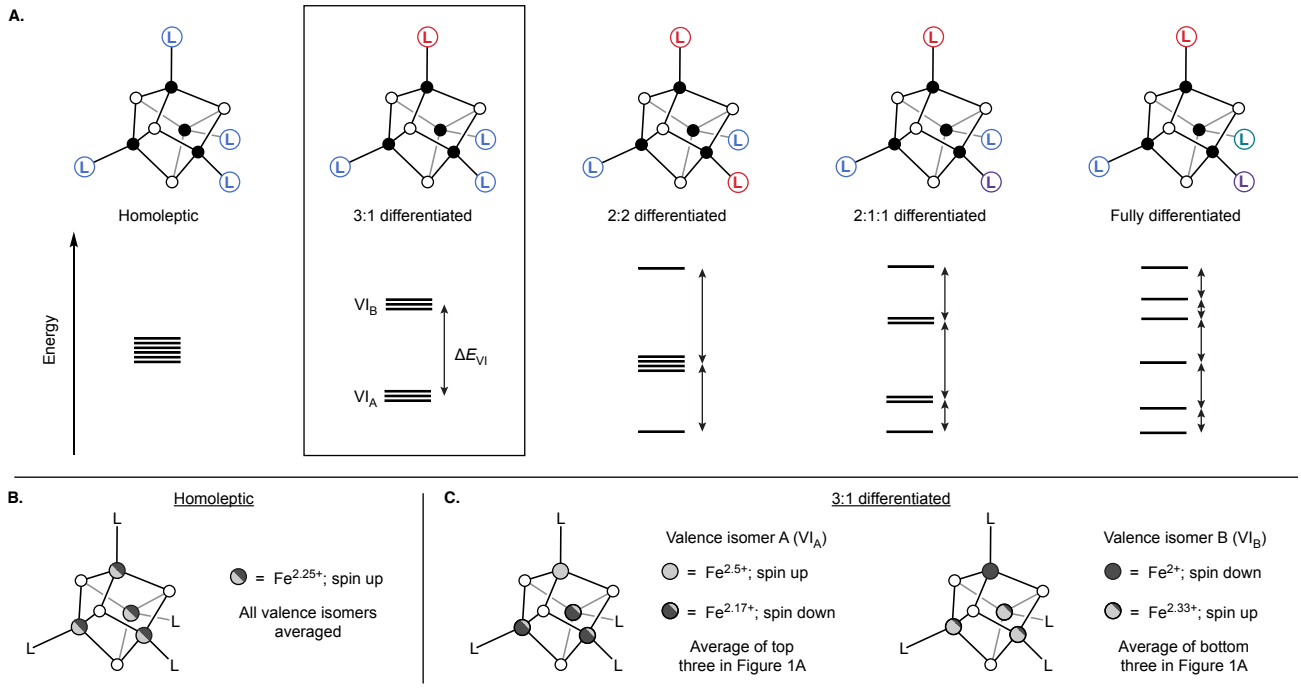

Figure 2. Effect of symmetry on the valence isomer landscape. Bottom panels highlight the effects of spin averaging in the homoleptic and 3:1 differentiated cases in the ground-state limit.

of each valence isomer are necessarily inequivalent (barring accidental degeneracy); there will always be, to some degree, preferential valence localization imbued by the different donor properties of the ligands binding the cluster. This accounts for why the ^{1}H NMR signals for the methylene protons in the homoleptic cluster $[Fe_4S_4(SBn)_4]^{3-}$ shift less than 2 ppm over a 100 °C range,[82] whereas the chemically analogous β-protons of the cysteine thiolates binding $[Fe_4S_4]^{1+}$ clusters in proteins frequently shift 5-10 ppm[83] over a much smaller temperature range (~25 °C).

In 3:1 symmetry, the deviation in the VT NMR behavior from that of a homoleptic cluster depends on the energy difference between VI_A or VI_B (Figure 2A and 2C). Simulations of the effects on the VT NMR spectra of increasing ΔE_{VI} are presented in Figure 3 using a model system with typical magnetic parameters (J = 80 cm^{-1}; $\Delta J_{34} = -\Delta J_{12} = J/6$; B = 6×$J$) and two NMR-active nuclei: one on the ligand bound to the unique site and one on the three ligands bound to the remaining sites, each with A_m = 0.1 MHz. Considering first the ligand bound to the unique Fe, we see that for $\Delta E_{VI} = 0$ (*i.e.*, the value for a homoleptic cluster), there is only a weak temperature dependence of the chemical shift, closely mimicking the behavior observed for real homoleptic systems (*vide infra*). Far more pronounced temperature dependencies are observed with the inclusion of even modest ΔE_{VI} values, as specific Fe sites within the cluster now spend more time experiencing minority or majority spin. As ΔE_{VI} approaches infinity, the NMR spectrum effectively reflects that of a single valence isomer. Thus, the temperature dependence of the NMR spectrum—its magnitude, direction, and curvature—is rich with information about the changing population of valence isomers, and therefore ΔE_{VI}.

These simulations also depict the effects of the valence averaging that occurs in 3:1 differentiated clusters. Specifically, for identical values of A_m, the magnitudes of the chemical shifts of the three identical ligands bound to the cluster core are significantly attenuated versus the chemical shifts for the unique site (Figure 3, right). This attenuation occurs because, on average, the three equivalent Fe sites consist of either one majority spin site and two minority spin sites (in VI_A), or two majority spin sites and one minority

spin site (Figure 2C). As the signals for the ligands bound to these sites are equivalent on the NMR timescale, the two spin orientations in each valence isomer oppose one another and thus attenuate δ_{para}, analogously to the phenomenon that gives rise to the near temperature-independence of the shifts of homoleptic clusters (*vide supra*).

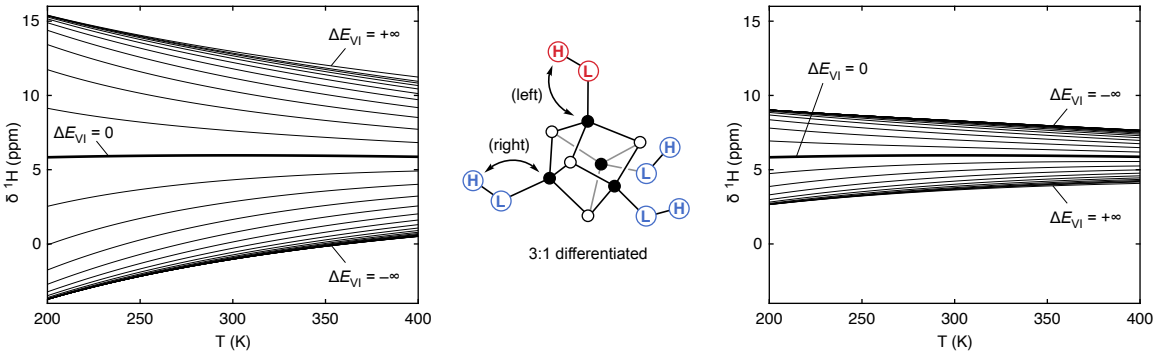

Figure 3. Simulated VT NMR traces for a 3:1 differentiated $[Fe_4S_4]^{1+}$ cluster freely equilibrating between different valence isomer states on the ^{1}H NMR timescale. Simulations for the proton on the ligand bound to the unique Fe sites and to the three equivalent Fe sites are shown in the left and right panels, respectively. Traces are contoured in 100 cm^{-1} between –1000 and 1000 cm^{-1}, as well as at ±∞. Magnetic parameters: J = 80 cm^{-1}; $\Delta J_{34} = -\Delta J_{12} = J/6$; B = 6×$J$; A_m = 0.1 MHz for both Fe^{2+} and Fe^{3+} for both protons.

2. Modeling the VT NMR Spectra of $[Fe_4S_4]^{1+}$ Clusters

We next describe our approach to extracting ΔE_{VI} and other magnetochemical properties from analysis of VT NMR data. Fits for the VT ^{13}C NMR data for a series of homoleptic $[Fe_4S_4]^{2+}$ clusters in the solid state have been reported, taking advantage of the high electronic symmetry of these systems,[84] but fits for the VT NMR data for $[Fe_4S_4]^{1+}$ or $[Fe_4S_4]^{3+}$ clusters of any symmetry are, to the best of our knowledge, absent from the literature (presumably because of their magnetic complexity). In addition to using rigorously 3:1 site-differentiated clusters (which have a simplified excited-state landscape with only two classes of valence isomers; *vide supra*), our approach toward overcoming the magnetic complexity of $[Fe_4S_4]^{1+}$ clusters can be summarized as follows:

- construction of a simplified magnetic exchange Hamiltonian,
- inclusion of solution-state magnetic data as an observable to be regressed upon, and
- numeric error estimation and independent model validation.

In discussing our choice of model Hamiltonian and the parameter relationships therein, we first point out that invoking the full "pair-of-pairs" Hamiltonian (Eq. 4) for a pair of valence isomers requires a total of eight independent Heisenberg J values and two independent B values (each valence isomer contributing four J values (parameterized as two J values and two ΔJ values) and one B value). Difficulties in fitting VT NMR data to more than two magnetic parameters for homoleptic $[Fe_4S_4]^{2+}$ clusters have been identified (though, partly due to $\Delta J/B$ covariance relationships that are not present in $[Fe_4S_4]^{1+/3+}$ clusters[84]) and suggest attempts at performing fits with ten free parameters are unlikely to succeed. In paring down the Hamiltonian, then, we began by ascribing to each valence isomer a global J value (J in Eq. 4). As previously defined, we adopt the convention that the energy of the lowest spin state of the valence isomer family with $Fe^{2.5+}$ at the unique site (VI_A) is zero, and we refer to the global J for this valence isomer as J_A. The global J for the second set of valence isomers (with a ferrous unique site) is then J_B. For both valence isomers, we take $\Delta J_{34} = -\Delta J_{12}$, reflecting the fact that antiferromagnetic exchange is stronger

between more oxidized Fe centers.[85] This property is general in $[Fe_4S_4]$ clusters, with global J values typically following the trend:

$$J([Fe_4S_4]^{3+}) > J([Fe_4S_4]^{2+}) > J([Fe_4S_4]^{1+})$$

(EQ. 7)

We assume further that ΔJ values have a fixed relationship to the global exchange coupling, *i.e.*, $\Delta J = J/n$, where the parameter n is equivalent for both valence isomers. As the effects of double exchange may be deconvolved from those of Heisenberg exchange in $[Fe_4S_4]^{1+}$ clusters,[84] we do treat double exchange, but with the assumption that it is of equivalent strength in both sets of valence isomer. Thus, the simplified Hamiltonian for the first valence isomer is

$$\widehat{H}_{VI_A} = J_A \sum_{1 \le m < n \le 4} \vec{S}_m \cdot \vec{S}_n \pm B\left(S_{34} + \frac{1}{2}\right) - \frac{J_A}{n}\left(\vec{S}_1 \cdot \vec{S}_2\right) + \frac{J_A}{n}\left(\vec{S}_3 \cdot \vec{S}_4\right)$$

(EQ. 8)

and that for the second valence isomer is

$$\widehat{H}_{VI_B} = J_B \sum_{1 \le m < n \le 4} \vec{S}_m \cdot \vec{S}_n \pm B\left(S_{12} + \frac{1}{2}\right) - \frac{J_B}{n}\left(\vec{S}_3 \cdot \vec{S}_4\right) + \frac{J_B}{n}\left(\vec{S}_1 \cdot \vec{S}_2\right)$$

(EQ. 9)

The interchange of spin labels $\vec{S}_1/\vec{S}_2$ with $\vec{S}_3/\vec{S}_4$ between Hamiltonians results from the change in physical location of the mixed-valence and diferrous pairs. We use these model Hamiltonians to calculate the *relative* energies of each spin state associated with each valence isomer, taking the ground state energy of $\widehat{H}_{VI_A}$ as 0 and the ground state energy of $\widehat{H}_{VI_B}$ as ΔE_{VI}.

With these assumptions, the exchange coupling parameter space has a total of four unique magnetic parameters over both families of valence isomers: J_A, J_B, n, and B. Each ligand nucleus studied

also contributes two hyperfine parameters: one for coupling to Fe^{2+} ($A_m(Fe^{2+})$) and an effective hyperfine coupling to $Fe^{2.5+}$ ($A_m(Fe^{2.5+})$), where

$$A_m(Fe^{2.5+}) = \frac{A_m(Fe^{3+}) + A_m(Fe^{2+})}{2}$$

(EQ. 10)

In attributing equal contributions of $A_m(Fe^{2+})$ and $A_m(Fe^{3+})$ to $A_m(Fe^{2.5+})$ for a fictitious, mononuclear $Fe^{2.5+}$ ion, Eq. 10 assumes that the electron is equally delocalized between the two mixed-valent Fe sites. This assumption is valid for most of the clusters studied herein (see SI), and although it likely does not hold for clusters with the most strongly donating X-type ligands (e.g. Bn, or N(H)Ph) in which the hole is expected to be partially localized at the site bound by the strong donor (and thus give rise to 'polarized double exchange'),[86–88] most effects of polarized double exchange are folded into the effective hyperfine coupling values. Specifically, the effective hyperfine values obtained for clusters where polarized double exchange occurs do not correspond to a pair of $Fe^{2.5+}$ hyperfine couplings, but rather to a pair of $Fe^{(2+n)+}$ and $Fe^{(3-n)+}$ couplings, where n is between 0 and 0.5. For the unique ligand, this introduces no error, and the observed hyperfine values are those corresponding to an Fe^{2+} coupling and a $Fe^{(3-n)+}$ ion. For the three identical ligands, the "$Fe^{2.5+}$" ion's effective hyperfine coupling is the weighted sum of the two true $Fe^{2.5+}$ ions in VI_B and the $Fe^{(2+n)+}$ ion in VI_A:

$$A_{m,eff}(Fe^{2.5+}) = \frac{1}{3} \times \left(2 \times A_m(Fe^{2.5+}) + A_m\left(Fe^{(2+n)+}\right)\right)$$

(EQ. 11)

Such deviations between $A_{m,eff}(Fe^{2.5+})$ and $A_m(Fe^{2.5+})$ for the three identical ligands are likely small and as such are not included in our model. Lastly, we do not fit the δ_{dia} values, and instead take δ_{dia} as the chemical shift of the corresponding nucleus on the protonated ligand (for the **1-X** series, excepting **1-SePh** and **1-**

TePh where we use $(PhSe)_2$ and $(PhTe)_2$) or the free ligand (for the [**1-L**]$^+$ series) in C_6D_6 solution. This further simplifies the fit parameter space.

Though the parameterization described above is simpler in terms of the number of parameters versus the full "pair-of-pairs" Hamiltonian previously described, it is still approximately twice as parameterized as previously implemented models.[84] This increase in number of parameters is partially offset by the greater effective information content of each ligand resonance in site-differentiated clusters. For a homoleptic cluster in which all Fe ions are equivalent on the NMR timescale, every ligand nucleus provides information on formally equivalent Fe ions, making them in a sense 'magnetically redundant' with every other ligand nucleus. In a 3:1 differentiated cluster, however, the ligand bound to the unique site provides complementary information with respect to the ligand nuclei on the three remaining sites in that the two classes of ligands report on magnetically distinct Fe ions. Additionally, we further increase the data-to-parameter ratio by including the solution-state magnetic moments for the cluster as an additional observation to refine against.

Operationally, models are generated as follows: 1) VT data (NMR and Evans method moments) are collected; 2) these data are input into a MATLAB implementation of the model described in the preceding paragraphs, with further information provided in the SI; 3) at least 20 independent fits are generated by drawing diamagnetic shift values from gaussian distributions centered on the assumed diamagnetic shift, with a variance of 0.1 ppm for ^{1}H nuclei and 30 ppm for ^{31}P nuclei, reflecting the modest degree of uncertainty associated with δ_{dia}; 4) these fits are compiled, and outliers with root mean square error (RMSE) greater than three times the standard deviation in population RMSE are rejected. Parameters for the remaining fits are then averaged to obtain the final parameters. Each fit is generated by searching the target function surface beginning with multiple starting points, identifying the minimum (or minima) and selecting the best overall fit. This procedure and the associated error analysis are discussed in more

detail in the Materials and Methods section and in the SI. The results of these fits are discussed in the following sections.

3. Cluster Synthesis and Characterization

In addition to 3:1 site-differentiation, we identified two other criteria for designing a system that would allow for the effects of ligand identity on valence isomerism in $[Fe_4S_4]^{1+}$ clusters to be quantitatively assessed: the cluster must have an easily tunable ligand sphere, and the cluster-bound ligands must have nuclei with sufficient spin density that they act as sensitive reporters for the magnetic moments within the clusters. We previously reported that the unsaturated *N*-heterocyclic carbene (NHC) IMes (1,3-dimesityl-imidazol-2-ylidene) both imparts robust 3:1 site differentiation and allows for a very wide range of ligands to be installed at the unique Fe site in $[Fe_4S_4]^{1+}$ clusters.[89–93] Thus, IMes satisfies the first of the design criteria. However, the paramagnetic part of the chemical shift for the backbone protons of IMes in a typical $[Fe_4S_4]^{+}$ cluster—here we take $(IMes)_3Fe_4S_4Cl$ as representative, with free IMes as the diamagnetic reference—is only −0.7 ppm at room temperature, making IMes spectroscopically undesirable as a ligand. We therefore turned to the saturated backbone congener of IMes, SIMes (1,3-dimesityl-imidazol-4,5-dihydro-2-ylidene),[94] which, as shown below, affords synthetically tunable, 3:1 site-differentiated $[Fe_4S_4]^{1+}$ clusters, and additionally features backbone protons with a strong paramagnetic response; for $(SIMes)_3Fe_4S_4Cl$ (**1-Cl**) the value of δ_{para} is 5.8 ppm in C_6D_6 solution at room temperature.

The syntheses of clusters of the form $(SIMes)_3Fe_4S_4X$ and $[(SIMes)_3Fe_4S_4L]^{+}$ are shown in Figure 4. Briefly, the thiolate, selenolate, and tellurolate complexes were obtained by treating the undifferentiated, homoleptic cluster $[Fe_4S_4(PCy_3)_4][BPh_4]$[65] with the tetraphenylphosphonium salt of the appropriate anion in slight excess (1.05-1.1 equiv) followed by treatment with SIMes (3.1 equiv) (Method A); **1-Cl** was prepared similarly using PPh_4Cl as the chloride source. The complexes **1-OPh**, **1-NHPh**, and **1-Bn**, were prepared by treating **1-Cl** with NaOPh, NaN(H)Ph, or BnMgCl, respectively (Method B). The cationic cluster $[\mathbf{1\text{-}NMI}]^{+}$ (NMI = *N*-methylimidazole) was prepared by treating $[Fe_4S_4(PCy_3)_4][BPh_4]$ with 3 equiv SIMes in THF, generating $[(SIMes)_3Fe_4S_4PCy_3]BPh_4$ *in situ*, followed

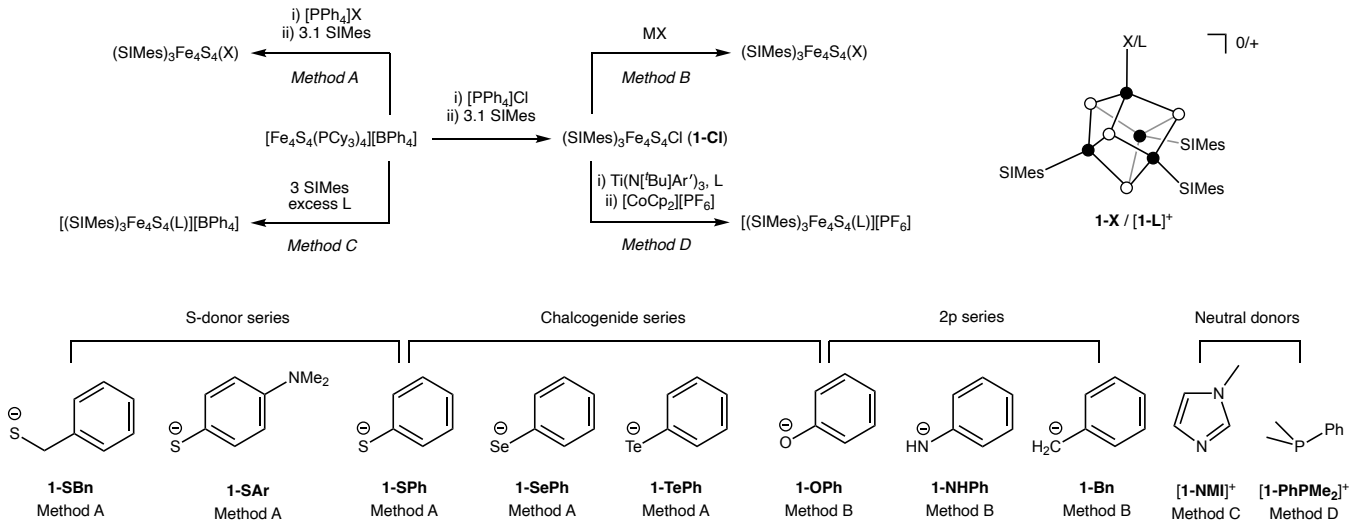

Figure 4. Synthesis of clusters **1-X** and [**1-L**]$^+$ beginning from $[Fe_4S_4(PCy_3)_4]BPh_4$. Full details are provided in the SI. SIMes = 1,3-dimesityl-imidazol-4,5-dihydro-2-ylidene; Ar′ = 3,5-dimethylphenyl.

by addition of excess *N*-methylimidazole, resulting in phosphine displacement to yield [**1-NMI**]BPh_4 (Method C). Access to the phosphine complex [**1-PhPMe$_2$**]$^+$ was afforded through the intermediacy of the all-ferrous cluster [**1-PhPMe$_2$**], which was prepared by Cl• abstraction from **1-Cl** using Ti(N[^{t}Bu]Ar)$_3$ (Ar = 3,5-dimethylphenyl)[91,92,95,96] in the presence of dimethylphenylphosphine. Oxidation of the resultant cluster with $[Cp_2Co][PF_6]$ in fluorobenzene afforded [**1-PhPMe$_2$**]$[PF_6]$ (Method D). All clusters adopt solution C_{3v} symmetry in their room-temperature (RT) NMR spectra (see SI). Those that were structurally characterized (**1-Cl**, **1-SPh**, **1-OPh**, **1-Bn**, **1-SAr** (Ar = 4-dimethylaminophenyl), **1-SBn**, and [**1-NMI**]BPh_4) display the expected pseudo-C_3 symmetry in the solid state (see Figure 5 for a representative

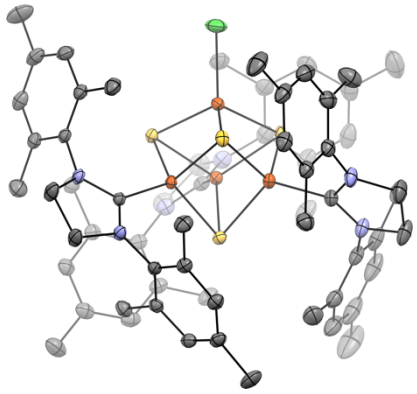

Figure 5. Thermal ellipsoid (50%) plot of **1-Cl**. Fe, orange; S, yellow; Cl, green; C, gray; N, blue. H-atoms and solvent molecules omitted for clarity.

example and the SI for the others) with parameters similar to those observed in members of the $(IMes)_3Fe_4S_4$ family.

The unique ligands in this series of clusters include π-donors, π-acceptors, and exclusive σ-donors, with free ligands whose conjugate acids span a range of nearly 40 pKa units. Within this set of compounds, several subsets may be defined, which we use as a basis for later comparisons:

- the 2p series, comprising **1-OPh**, **1-NHPh**, and **1-Bn**;
- the chalcogenide series, composed of **1-OPh**, **1-SPh**, **1-SePh**, and **1-TePh**;
- the thiolate (S-donor) series, including **1-SPh**, **1-SAr**, and **1-SBn**, each having $^{-}$SR ligation but with variable R groups; and
- those with neutral donors, [**1-NMI**]$^{+}$ and [**1-PhPMe$_2$**]$^{+}$.

The ligand diversity espoused by these series is captured by, among other metrics, the electrochemical properties of the clusters whose $[Fe_4S_4]^{1+/2+}$ couples (vs. Fc/Fc^{+}) in ortho-difluorobenzene (DFB) range from −1.46 V for **1-Bn** to −1.23 V for **1-TePh** within the **1-X** series and up to −0.74 V for [**1-PhPMe$_2$**]$^{+}$ (Figure 6). The compounds described in this section have additionally been fully characterized by a suite of other methods, including IR, UV-Vis, and EPR spectroscopy; these results are collected in the SI.

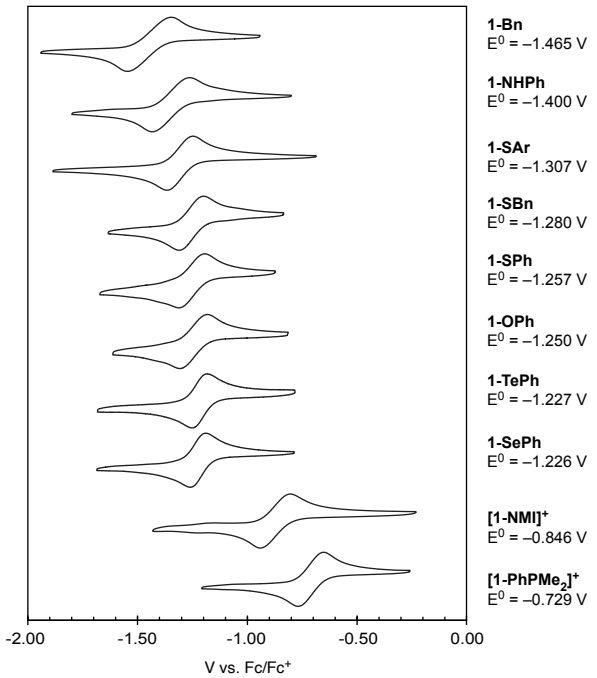

Figure 6: Cyclic voltammograms for the **1-X**/[**1-L**]$^+$ series in DFB containing 500 mM $TBAPF_6$, ordered from lowest to highest potential (vs. Fc/Fc^+).

4. Qualitative Analysis of VT ^{1}H NMR Spectra and Magnetic Moments

We first qualitatively compare the VT magnetism of compounds **1-X/[1-L]$^+$** with analogous homoleptic $[Fe_4S_4(SR)_4]^{3-}$/$[Fe_4S_4(PR_3)_4]^+$ complexes, as well as with their protein-bound $[Fe_4S_4]^{1+}$ counterparts ligated by four Cys thiolates. The room-temperature (RT) magnetic moments of the **1-X** series fall between 3.0-3.6 μ_B. Similar values have been reported for the room temperature magnetic moments of $[Fe_4S_4(SBn)_4]^{3-}$ and $[Fe_4S_4(SPh)_4]^{3-}$ (~3.7 and ~3.6 μ_B, respectively)[69], *B. polymyxa* Fd_{red} (3.2 μ_B),[97] and the reduced 4Fe ferredoxin from *D. gigas* (4.0 μ_B).[98] The magnetic moments for [**1-NMI**]BPh_4 and [**1-PhPMe$_2$**]PF_6 are 3.4 and 4.2 μ_B, respectively; the somewhat high value for [**1-PhPMe$_2$**]PF_6 is similar to that reported for the related cluster $[Fe_4S_4(P^tBu_3)_4][BPh_4]$ (μ_{eff} = 4.19 μ_B at 297 K)[65] and suggests that phosphine coordination weakens magnetic exchange interactions (thus giving rise to larger room-temperature magnetic moments). Overall, these comparisons demonstrate that carbene ligation minimally affects the gross magnetic properties of the $[Fe_4S_4]^{1+}$ core relative to thiolate-ligated variants, and therefore that clusters **1-X/[1-L]$^+$** are electronically similar to $[Fe_4S_4]^{1+}$ clusters with more traditional ligand spheres.

The VT ^{1}H NMR spectra of all clusters have been measured between room temperature and approximately −90 °C in either d_8-toluene (for neutral compounds), d_8-THF (for [**1-NMI**]BPh_4), or d_2-DCM (for [**1-PhPMe$_2$**]PF_6, which is in equilibrium with [**1-THF**]PF_6 when dissolved in THF; see SI). At RT, the NMR spectra exhibit typical patterns of spin delocalization/polarization, indicating (importantly) that contact shifts dominate δ_{para}.[68] For example, a large, positive chemical shift (87 ppm) is observed for the benzylic protons in **1-SBn**. Similarly, the benzylic protons of **1-Bn** and the N-H proton of **1-NHPh** have large, positive chemical shifts (256 and 199 ppm, respectively), indicative of direct spin delocalization through the σ-bonding framework (in addition to π-type delocalization via the S lone pairs in **1-SBn**).[99] As is typical for systems experiencing π-delocalization,[68,100] the aryl groups of **1-NHPh**, **1-OPh**, **1-SPh**, **1-SAr**, **1-SePh**, and **1-TePh** exhibit alternating patterns for the ^{1}H nuclei, with the *ortho*-

and *para*-protons appearing upfield and the *meta*-protons downfield relative to their typical diamagnetic frequencies (Figure 7).

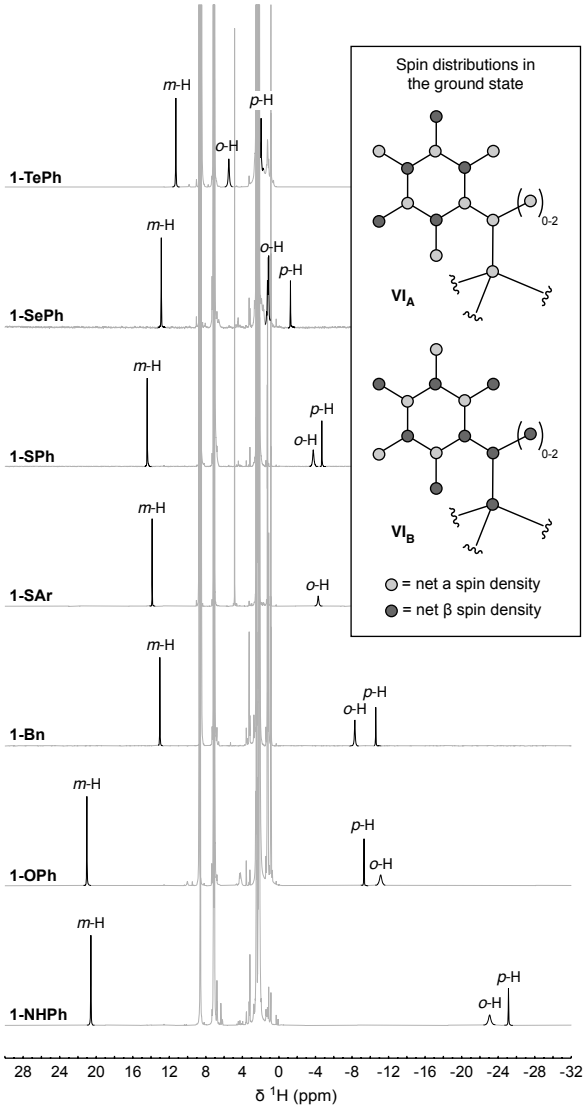

Figure 7. Portions of the 500 MHz ^{1}H NMR spectra of selected compounds showing the paramagnetically shifted aryl resonances. *Inset*: Typical spin delocalization pattern for phenyl groups bound to high-spin Fe centers through an intermediate atom or group E.

In this series, the largest paramagnetic aryl shifts are observed for **1-NHPh**, followed by **1-OPh**, **1-SPh/1-SAr**, **1-SePh**, and **1-TePh** (Figure 7). Despite the lack of a lone pair on the benzyl moiety, **1-Bn** exhibits the same pattern of shifts in the benzylic phenyl, though the magnitude of the shifts in this compound are somewhat attenuated relative to the remainder of the 2p series. While the magnitude of the hyperfine coupling tracks with the extent to which the lone pair on the ligand is energetically and spatially

matched with the phenyl π-system and the Fe *d*-manifold, it also reflects the relative population of the two valence isomers (*vide supra*); these effects have different temperature dependencies, and they can therefore be deconvoluted by modeling the VT NMR spectra as described below.

All paramagnetically shifted resonances of the compounds prepared in this work generally show Curie-type behavior, though nonlinearity is observed to varying extents when plotted vs. 1/T (see SI), reflecting the fact that Fe–S clusters generally cannot be expected to strictly obey the Curie law on account of their many low-lying thermally populated electronic states. The subtle curvature of these traces contains a wealth of information regarding the population of various excited states, and ultimately forms the basis upon which these spectra may be quantitatively interpreted as described in the following section.

Comparison of the VT ^{1}H NMR spectra of **1-SPh** (where $\Delta E_{VI} \neq 0$, owing to the 3:1 site-differentiation pattern) with those of the related homoleptic complex $[Fe_4S_4(S(^{m}Tol))_4]^{3-}$ (where $\Delta E_{VI} = 0$ on account of the homoleptic ligand sphere) reveals the dramatic effects of valence isomerism. We first note that the solution VT magnetic moments of the homoleptic aryl thiolate complex $[Fe_4S_4(SPh)_4]^{3-}$ and **1-SPh** are nearly identical (Figure 8, upper panel), and we expect the same to be true for $Fe_4S_4(S(^{m}Tol))_4]^{3-}$ (VT magnetic moment data were not reported for the latter, and VT NMR data were not reported for $[Fe_4S_4(SPh)_4]^{3-}$);[69] thus, the nature of the coupling and the magnitude of the *J* values in all three clusters are likely to be very similar to one another. However, the NMR chemical shifts of the *para* protons of $[Fe_4S_4(S(^{m}Tol))_4]^{3-}$ are nearly temperature-independent, shifting on average ~2×10^{-3} ppm K^{-1}, whereas the analogous *para* proton of **1-SPh** shows a significant temperature dependence, shifting on average ~28×10^{-3} ppm K^{-1}—more than an order of magnitude larger (Figure 8, lower panel). The pronounced temperature dependence of the proton resonances in **1-SPh** is a result of partial valence localization by the thiophenolate ligand that arises from the disparities in the donor/acceptor properties of SIMes and thiophenolate (analogous to the predictions from the generic simulations in Figure 3). This temperature dependence of chemical shifts is borne out for every cluster studied in this work, and is in stark contrast

with the near temperature-independence of shifts observed for proton resonances of homoleptic, thiolate ligated $[Fe_4S_4]^{1+}$ clusters.[69]

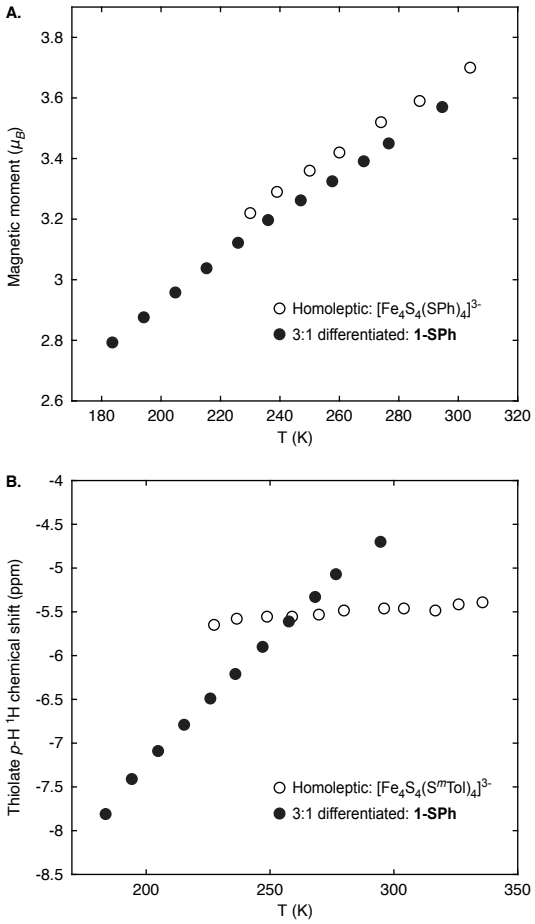

Figure 8. Magnetochemical comparisons of homoleptic and 3:1 differentiated clusters. A) Solution-state magnetic moments for $[Fe_4S_4(SPh)_4]^{3-}$ in CD_3CN and **1-SPh** in toluene-d_8 versus temperature. Data on the former taken from Table III in ref. 69. B) Plot of the chemical shift of the aryl thiolate *para*-H for $[Fe_4S_4(S^mTol)_4]^{3-}$ in CD_3CN and the thiophenolate *para*-H for **1-SPh** in toluene-d_8 versus temperature. Data on the former extracted from Figure 6 in ref. 69.

*5. Representative Quantitative Analysis of **1-SPh***

For **1-SPh**, four ^{1}H NMR resonances—the *ortho*, *meta*, and *para* protons on the thiophenolate ligand, and the SIMes backbone methylene protons—display significant paramagnetic shifting (Figure 9A and 9B) and were used in the fitting protocol described above; the magnetic moment data (Figure 9C) were also employed. We obtained an average fit value for ΔE_{VI} of 53 ± 26 cm^{-1}, meaning that the ground-state valence isomer is VI_A, with preferential localization of $Fe^{2.5+}$ at both the unique site and its double-exchange-coupled partner, and that the ground S = 1/2 state associated with VI_B (in which Fe^{2+} occupies the unique site) is not much higher in energy. This finding also demonstrates that, at least in the context of the [(SIMes)$_3$Fe$_4$S$_4$] series, the moderate σ- and π-donor ligand SPh^- is a somewhat stronger overall donor than SIMes (a strong σ donor and a weak π acceptor).

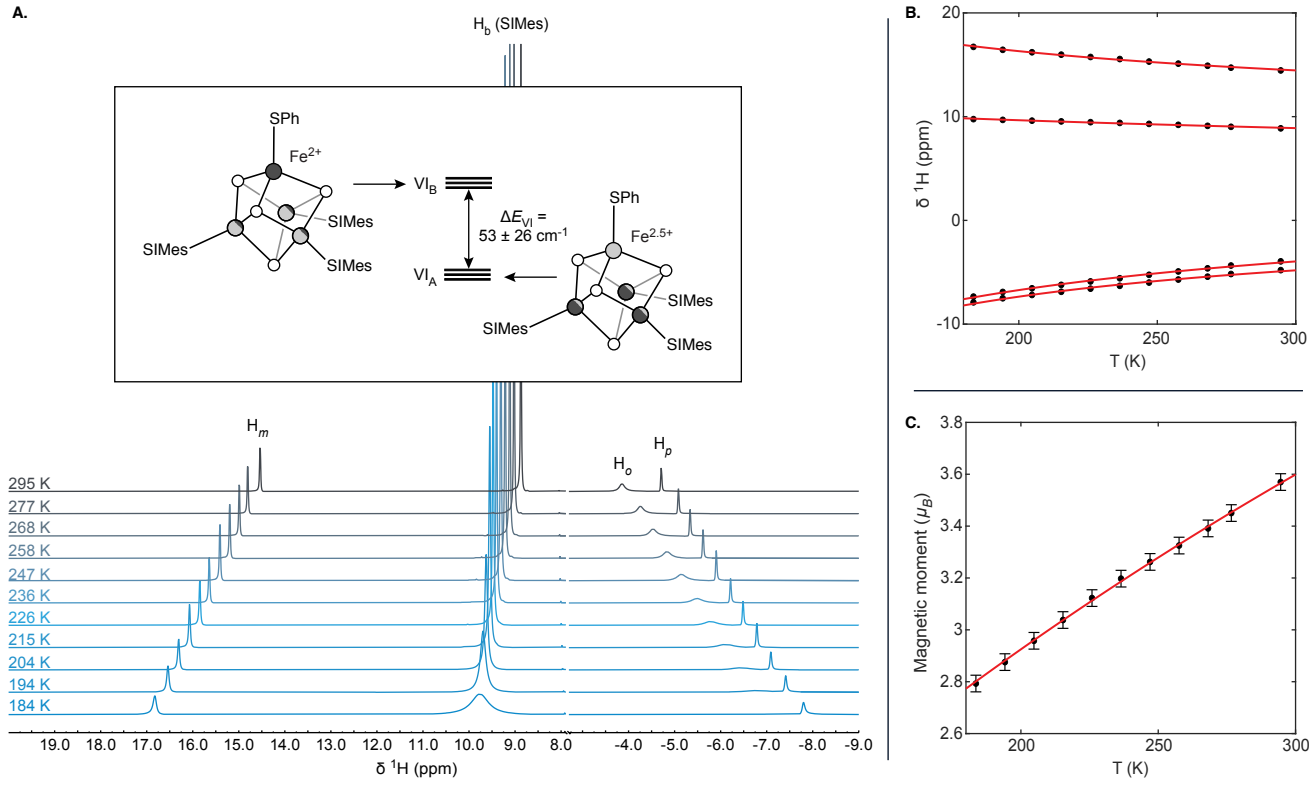

Figure 9. Data and fits for **1-SPh**. A) Paramagnetic regions of the VT NMR spectra of **1-SPh** in toluene-d$_8$ between RT and 184 K, with depiction of the ground and excited valence isomer states for **1-SPh**. B) Plot of the VT ^{1}H carbene backbone and aryl thiolate shifts of **1-SPh** (black points) and global best fit of the data (red trace). C) Evans-method magnetic moments for **1-SPh** (black points) and best global fit of the data (red trace).

The global J values for the two valence isomers are similar (J_A = 97 ± 6 cm^{-1} and J_B = 80 ± 7 cm^{-1}), and compare well to reported (or estimated) J values for $[Fe_4S_4]^{1+}$ clusters, which typically lie in the range 80-120 cm^{-1},[6,21,101,102] though this comparison is perhaps only of qualitative utility as many of these J values have been derived from fits that ignore double exchange, or that use slightly different exchange Hamiltonians. The modeled B value is 660 ± 70 cm^{-1}, and all other B values determined in this work lie between 500-1000 cm^{-1} (excepting that for [**1-PhPMe$_2$**]$^+$; see SI). The observation of B values between 500 and 1000 cm^{-1} is noteworthy as the magnitude of the double exchange parameter for cuboidal Fe–S clusters has been a prior topic of debate in the literature.[31,84,87,103–105] Our findings, along with the more contemporary work,[84,106] support the idea that the effective B values for the mixed valence pairs in $[Fe_4S_4]$ clusters are on the order of several hundred wavenumbers, though it has been pointed out that B values for even simple mixed valence compounds are somewhat ill-defined on account of the multi-orbital nature of double exchange in these systems;[27] the latter proposal may in part account for the observed spread in B values amongst the clusters studied herein (see SI). We find for the parameter n a value of 5.6, which is very similar to the value of 5 that may be inferred for the related thiolate-ligated $[Fe_4S_4]^{1+}$ cluster $(Et_4N)_3[Fe_4S_4(SPh)_4]$ ($J(Fe^{3+}–Fe^{2+})$ = 120 cm^{-1} and $J(Fe^{2+}–Fe^{2+})$ = 80 cm^{-1};[21] this can be re-parameterized as J = 100 cm^{-1} and ΔJ = 20 cm^{-1}, with n = 100/20 = 5). Overall, the strong agreement between the magnetic parameters obtained by modeling the VT NMR data of our complexes with those obtained for other synthetic and biogenic $[Fe_4S_4]^{1+}$ clusters supports the accuracy of the parameters obtained in our modeling procedure, including the ΔE_{VI} values (which have not been quantitatively determined in other systems).

The relatively low magnitude of $|\Delta E_{VI}|$ for **1-SPh** would suggest that there should be appreciable population of both VI_A and VI_B even at the low temperatures amenable to EPR detection (< 40 K), as has been observed in HiPIPs[44,107] and in photo-oxidized/reduced synthetic $[Fe_4S_4]$ clusters.[108–111] Indeed, **1-SPh** exhibits a major and a minor signal in its EPR spectrum (see SI), with the minor signal growing at

the expense of the major signal at higher temperatures; such behavior is inconsistent with a physical mixture of non-interconverting spin systems (*e.g.*, different conformations or contamination by a minor impurity) and is instead consistent with a ground-excited state relationship between the two observed $S = 1/2$ species. We propose that these species are the ground states of the two valence isomers, VI_A (major) and VI_B (minor). This interpretation is further supported by the observation that only for clusters with small $|\Delta E_{VI}|$ values such as **1-SPh** is this behavior observed; clusters with large $|\Delta E_{VI}|$ values—**1-Bn** and **1-NHPh**—exhibit a single $S = 1/2$ EPR signal (see SI), as expected for population of a single valence isomer.

Although ΔE_{VI} could in principle be measured by analyzing the VT EPR spectra (assuming a two-state Boltzmann distribution), there are some limitations to this approach. First, the relaxation properties of the two signals could be different (this is true in certain HiPIP systems[112]), and any such differences would complicate a Boltzmann-type analysis. Second is the obvious ambiguity in the sign of ΔE_{VI}; while in some cases it is possible to identify two $S = 1/2$ species by CW EPR, it is not possible to directly assign which corresponds to VI_A or VI_B, and thus to determine if ΔE_{VI} is positive or negative. Third is that the EPR data must be acquired at low temperature, and as a result only clusters that have small $|\Delta E_{VI}|$ values will have observable population of the higher-energy valence isomer in this temperature regime. In contrast, obtaining ΔE_{VI} values by fitting NMR data allows for a wider range of clusters to be analyzed because, near ambient temperature, there is appreciable population of states that are 10^2-10^3 cm^{-1} higher in energy than the ground state. Fourth, in frozen solutions, spectra can be complicated by the presence of a physical mixture of non-interconverting states (*e.g.*, more than one conformation, as we observe for **1-SBn**; see SI); such complications arising from conformational dynamics are circumvented in ambient-temperature, solution ^1H NMR spectroscopy because of rapid conformational averaging on this timescale. Fifth is the broad linewidths of the EPR spectra of $[Fe_4S_4]^{1+}$ clusters, which requires that that the two signals have sufficiently different *g* tensors in order to be resolved; such considerations may explain why

we only observe a single signal for a few clusters with relatively small $|\Delta E_{VI}|$ values (see SI). Lastly, EPR analysis alone does not allow for the nature of the observed excited states to be distinguished; for low offset energies ($\Delta E_{EPR} < J$) it can be reasonably inferred that observed low lying states are most likely excited valence isomer states, but when ΔE_{EPR} approaches the magnitude of spin ladder spacings ($\Delta E_{EPR} \approx J$) it becomes less clear whether observed excited states are excited valence isomer states or excited spin states for one valence isomer.

*6. Comparison of ΔE_{VI} across the **1-X**/[**1-L**]$^+$ series*

The ΔE_{VI} values were determined for ten members of the **1-X**/[**1-L**]$^+$ series (depicted at the bottom of Figure 4). Plots of the VT NMR data with associated fits are provided in Figure 10 and the results are presented in Table 1 and Figure 11. For each member of the *S*-donor series, ΔE_{VI} is uniformly positive, increasing from 53 ± 26 cm^{-1} (**1-SPh**) to 70 ± 25 cm^{-1} (**1-SAr**) and 150 ± 50 cm^{-1} (**1-SBn**). The observed trend is chemically reasonable because the electron-donating *p*-NMe_2 group in **1-SAr** should stabilize $Fe^{2.5+}$ at the unique site relative to the *p*-H atom in **1-SPh**, and the benzyl substituent in **1-SBn** is likewise more donating than either aryl substitution in the other two complexes (as supported, for example, by the lower $[Fe_4S_4]^{1+/2+}$ redox couple for $[Fe_4S_4(SBn)_4]^{2-/3-}$ compared with $[Fe_4S_4(SPh)_4]^{2-/3-}$ and by the pK_as of

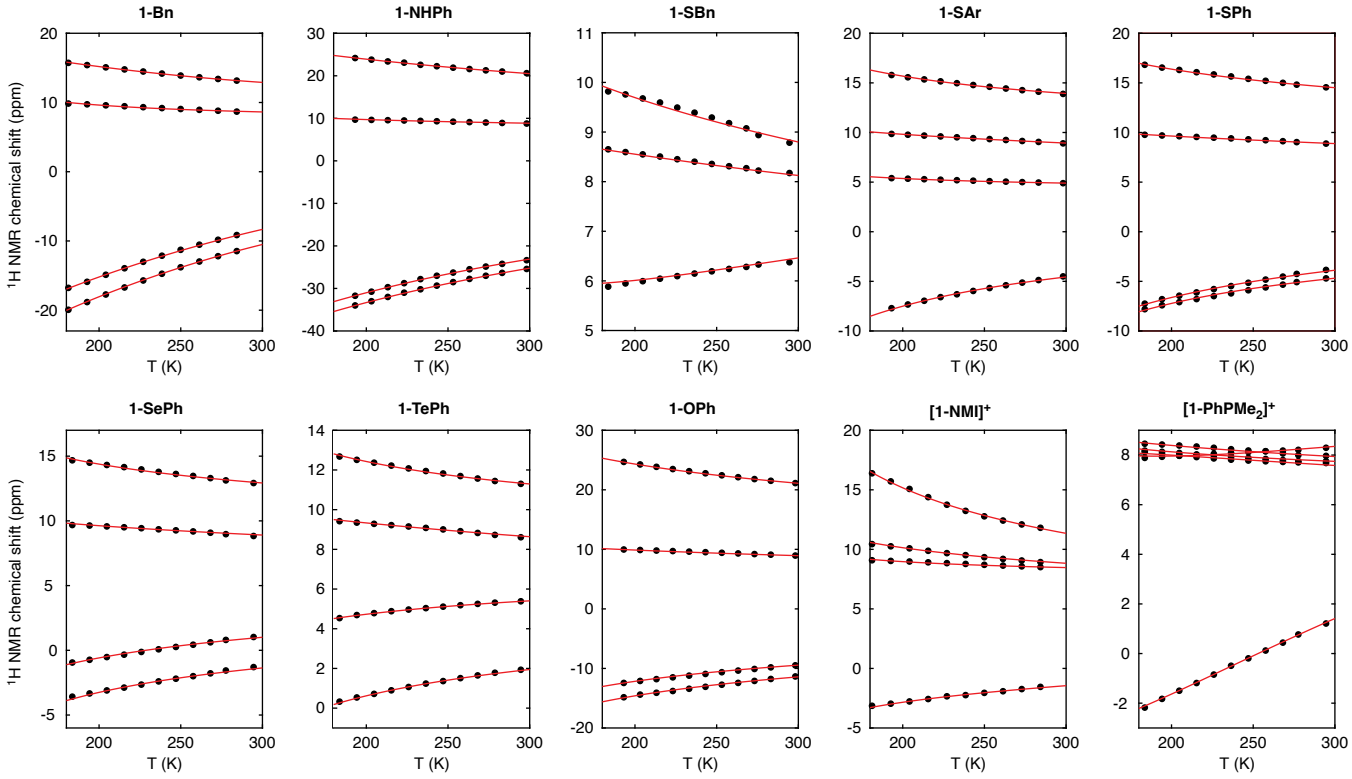

Figure 10. Plots of the VT NMR data (black points) for the ten clusters analyzed herein with associated best global fits (red traces). VT magnetic moment data (see SI) were also collected and fit. The benzylic protons in **1-Bn**, the anilido proton in **1-NHPh**, the benzylic protons in **1-SBn**, and the phosphine ^{31}P in [**1-PhPMe$_2$**]$^+$ were also included in the fits but are not shown here for clarity (see SI).

Table 1: Tabulated magnetic energetic parameters for the **1-X/[1-L]$^+$** series, as determined by VT NMR analysis.

Compound	ΔE_{NMR} (cm^{-1})
1-Bn	680 ± 100
1-NHPh	470 ± 85
1-SBn	150 ± 50
1-SAr	70 ± 25
1-SPh	53 ± 26
1-SePh	43 ± 26
1-TePh	39 ± 27
1-OPh	20 ± 26
[1-NMI]$^+$	−57 ± 35
[1-PhPMe$_2$]$^+$	−270 ± 40

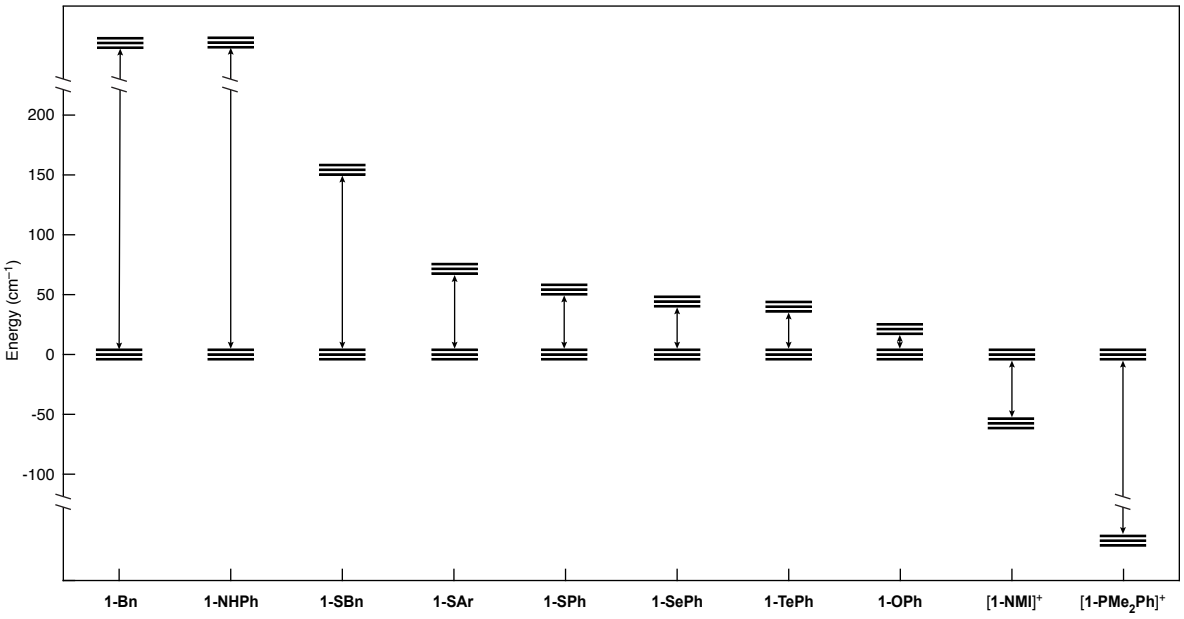

Figure 11. Graphical depiction of the ground valence isomer states for the compounds studied by VT NMR in this work. ΔE_{VI} values are taken from Table 1 and the energy of the ground state of VI_A is taken to be zero.

the protonated thiolates; see SI and below).[3] The range in thiolate ΔE_{VI} values (on the order of 10^2 cm^{-1}) is similar to the offset energy ranges that have been computed for the Cys_4-ligated $[Fe_4S_4]^{3+}$ clusters in *E. halophila* and *C. vinosum* HiPIPs using a simple electrostatic model of 56 – 113 cm^{-1} and 16 – 65 cm^{-1}, respectively.[8]

The members of the chalcogenide series (**1-SPh**, **1-SePh**, and **1-TePh**) are relatively uniform in their ΔE_{VI} values (Table 1), while the 2p series (**1-OPh**, **1-NHPh**, **1-Bn**) exhibits a large range of ΔE_{VI} values: 20 ± 26 cm^{-1} (**1-OPh**), 470 ± 90 cm^{-1} (**1-NHPh**), and 680 ± 100 cm^{-1} (**1-Bn**). The particularly large ΔE_{VI} values for **1-NHPh** and **1-Bn** are a consequence of the exceptional donor strengths of the anilide and benzyl ligands. Similarly, we have previously observed that alkyl groups localize Fe^{3+} when weaker donors complete the coordination sphere of $[Fe_4S_4]^{2+/3+}$ clusters,[88,113] and the present work both quantifies this phenomenon and extends it to the $[Fe_4S_4]^{1+}$ state. Our analysis also shows that anionic *N*-donors (both strong σ and π donors) have similar localizing power to hydrocarbyl fragments (exceptionally strong σ donors, with minimal π bonding). Indeed, at room temperature, the extent of $Fe^{2.5+}$ localization in **1-NHPh** is in fact greater than that in **1-Bn** when also accounting for differences in the magnetic structures of each valence isomer (*vide infra*). Such observations may inform on the electronic structures of intermediates in biological nitrogen fixation.

The hyperfine values for the thiolate proton resonances bound to $[Fe_4S_4]$ clusters have been extensively studied, and in general exhibit a Karplus-type relationship between measured hyperfine coupling and Fe-S-C-H dihedral angle.[66,76,111,114–116] The dihedral dependence of the effective mononuclear benzylic proton hyperfine couplings (A_m values) to $Fe^{2.5+}$ ions in a single crystal of $[Fe_4S_4(SBn)_4]^{3-}$ have been determined and take the following form:[111]

$$A_m(\theta) \approx 1.391 - 0.227\cos(\theta) - 0.143\cos^2(\theta)$$

(EQ. 12)

Here, $A_m(\theta)$ is the isotropic mononuclear hyperfine coupling of the benzylic proton to the proximal $Fe^{2.5+}$ ion, in MHz, as a function of the Fe-S-C-H dihedral angle θ. The average value of this function over all dihedral angles is 1.32 MHz, and may be directly compared with the $A_m(Fe^{2.5+})$ value obtained for **1-SBn** in this work of 0.98 MHz. The close agreement of these two independently determined parameters further attests to the accuracy of the parameters obtained in this work, with possible differences being attributable

to dihedral angle preferences and slightly different bonding situations between the two clusters (*e.g.*, differences arising from NHC ligation).

All complexes discussed thus far feature X-type ligands and exhibit $\Delta E_{VI} > 0$, indicating at least some favorability for localizing $Fe^{2.5+}$ at the unique site. The neutral donor complexes ([**1-NMI**]$^+$ and [**1-PhPMe$_2$**]$^+$) break this trend with negative ΔE_{VI} values (-57 ± 35 cm^{-1} and -270 ± 40 cm^{-1}, respectively), meaning that the ground-state valence isomer for both complexes is that with an Fe^{2+} ion at the unique site (VI_B). The very low ΔE_{VI} value for [**1-PhPMe$_2$**]$^+$ can be attributed to the π-accepter properties of the phosphine ligand. Similar valence localization behavior (*i.e.*, a preference for localizing Fe^{2+}) has been qualitatively observed in alkene and alkyne adducts of $[Fe_4S_4]^{1+}$ cluster cores,[92] and the current results substantiate the prior findings while also providing quantitative insights into the energy differences between the valence isomers.

For the complete series, we find a strong, positive correlation between the DMSO pK_a of the conjugate acid of the ligand to the unique Fe site (XH or [LH]$^+$) and ΔE_{VI} (Figure 12A). Although pK_a is only a crude proxy for a ligand's donor strength (the latter will additionally depend on the nature of the σ and π bonding), this finding is consistent with the expectation that stronger donors at the unique site will tend to favor VI_A. Similarly, ΔE_{VI} increases with decreasing $[Fe_4S_4]^{1+/2+}$ redox potential (Figure 12B); with increasing donicity of the ligand bound to the unique Fe, the cluster becomes more reducing and the favorability of localizing $Fe^{2.5+}$ at the unique Fe should likewise increase. Although the observed trend is qualitatively sensible, the relationship between the $[Fe_4S_4]^{1+/2+}$ redox potential and ΔE_{VI} is likely more complicated because altering the unique ligand will change the nature of the redox-active orbital in both valence isomers as well as the relative populations of the valence isomers (all of which is averaged on the CV timescale). As a result, the extent to which the unique Fe is involved in redox chemistry will be different in each cluster as will the energies of the unique Fe's orbitals, and these effects on the redox potential cannot be decoupled.

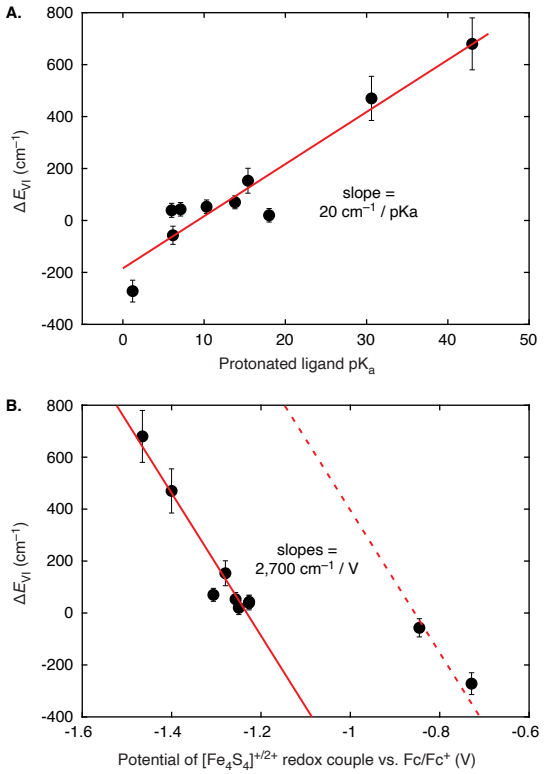

Figure 12. Molecular basis for trends in ΔE_{VI} values. A) Plot of ΔE_{VI} values versus DMSO pK_a values for the X-H species (for the **1-X** series) or $[L\text{-}H]^+$ (for the $[\mathbf{1\text{-}L}]^+$ series). Values for pK_a were corrected for solvent differences where necessary.[117–122] The pK_a value for PhTeH is estimated as 6 (pK_a values for $HESi(SiMe_3)_3$ in $MeC(O)^tBu$ are 8.3 (E = Se), and 7.3 (E = Te)[123]—this relative pK_a difference has been applied using the pK_a value of PhSeH as a reference). The red trace is a linear best fit for the dataset and intended to guide the eye. B) Plot of ΔE_{VI} values versus $[Fe_4S_4]^{1+/2+}$ couple in DFB/$TBAPF_6$. The solid red trace is the linear best fit for the **1-X** series, and the dashed red trace is the same line shifted horizontally by 0.38 V to empirically account for the shift in redox potential associated with the charge state change between the **1-X** series and the $[\mathbf{1\text{-}L}]^+$ series.

7. Magnetochemistry as a Determinant of Valence Distribution

A facet of the valence isomer problem that emerges for $[Fe_4S_4]^{1+}$ clusters is the dependence of the valence electron distribution on the spacings of the spin ladders for each valence isomer, especially at ambient temperature. That is, a valence isomer is not simply a single $S = 1/2$ state with a particular geometrical distribution of $Fe^{2.5+}$ or Fe^{2+} ions within a $[Fe_4S_4]^{1+}$ cluster, but rather an ensemble of different thermally accessible spin states all sharing a common valence pattern. The population of a valence isomer at a given temperature is, therefore, given by the extent to which any spin state, ground or excited, with that valence electron configuration is populated. Thus, although we have used ΔE_{VI} as a convenient way to parameterize valence isomerism, a more complete picture requires consideration of the spin ladders of each valence isomer, particularly in instances where $J \leq k_B T$.

To illustrate this point, we present the spin ladders—partitioned by valence isomer—for [**1-NMI**]$^+$, **1-SPh**, and **1-SBn** (Figure 13). Each cluster features a dense manifold of excited states, many of which are sufficiently low in energy and/or high in multiplicity to be extensively populated at room temperature. For [**1-NMI**]$^+$, VI_B is the ground-state valence isomer, but the spin ladder of VI_A is more compressed (primarily because $J_A < J_B$), and therefore the population of VI_A in the high-temperature limit should be higher than would be predicted based on only the magnitude of ΔE_{VI}. Indeed, at 298 K, the computed population of VI_A is 55% when taking into account the entire spin ladder, whereas a value of 43% is calculated when considering only a two-level system comprised of the ground states of each valence isomer.

The deviations from two-level type behavior for all compounds studied in this work are plotted in Figure 14A in terms of the parameter η, which we define as the difference between the $\%VI_A$ population as calculated using the full spin ladder and the $\%VI_A$ population computed for a two-level model with ΔE_{VI} as the difference in energy between states:

$$\eta = \%VI_A(full\ ladder) - \%VI_A(two - level)$$

(EQ. 13)

Such deviations are up to ~10% at RT (Figure 14B), and achieving similar differences in occupation by varying ΔE_{VI} alone would require changing ΔE_{VI} values by up to 40 cm^{-1} (assuming initially $\Delta E_{VI} \approx 0$). Numerically, this value is on the order of many ΔE_{VI} values we have measured, and it is therefore important to consider the thermal population of the spin ladder when considering the phenomenon of valence isomerism (see SI for analogous plots from Figure 12 that take into account this consideration). However, it must be emphasized that ΔE_{VI} is nonetheless a reliable parameter, even if the valence electron configuration for a 3:1 differentiated $[Fe_4S_4]^{1+}$ resists description by a single parameter. Thus, considering

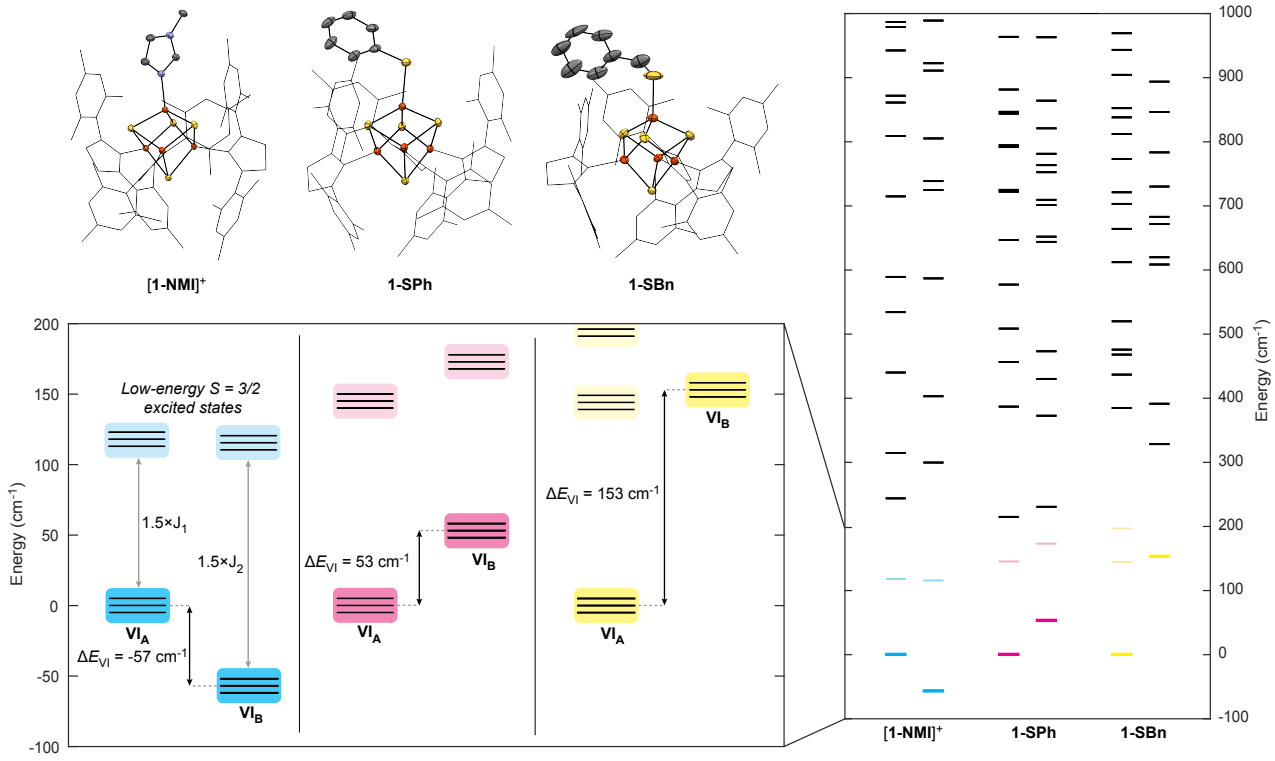

Figure 13. *Upper, left to right*: Solid state structures of [**1-NMI**]$^+$, **1-SPh**, and **1-SBn**, with thermal ellipsoids contoured at 50% and color scheme as in Figure 5. Counterions and hydrogen atoms are omitted for clarity, and SIMes ligands are shown in wireframe. *Lower left*: States on the spin ladders of [**1-NMI**]$^+$, **1-SPh**, and **1-SBn** for both valence isomers with energies below 200 cm^{-1} (relative to VI_A, which is arbitrarily set to zero), graphically showing the difference in valence isomer energies, and the energies of the first low lying excited $S = 3/2$ state computed from Hamiltonians Eq. 8 and Eq. 9 in terms of J_1 and J_2 using values obtained from VT NMR fits. *Right:* Low-energy (<1000 cm^{-1}) spin ladders for [**1-NMI**]$^+$, **1-SPh**, and **1-SBn**, partitioned by valence isomer, as computed from Hamiltonians Eq. 8 and Eq. 9 using parameters obtained from VT NMR fits. States colored cyan, magenta, and yellow correspond to states set out in the lower left panel.

ΔE_{VI} is necessary, but not sufficient, in accurately describing the valence electron distribution of an $[Fe_4S_4]^{1+}$ cluster at or near ambient temperature.

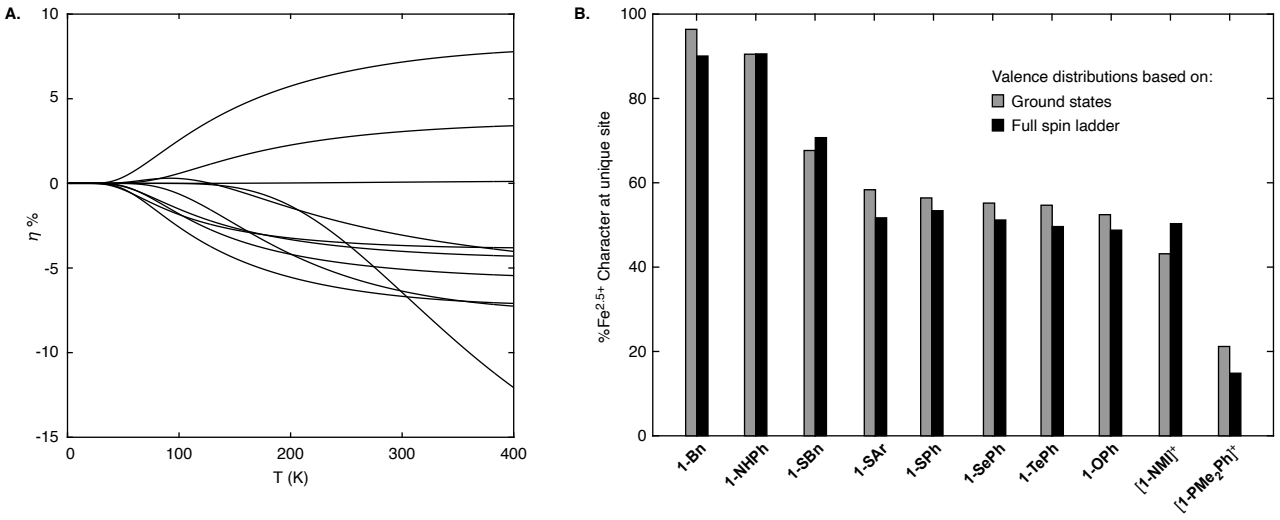

Figure 14. Differences between the computed valence distributions when considering only the ground-state valence isomers and the full spin ladder. A) Plot of η as a function of T for all compounds studied in this work. B) Bar plot showing the population of VI_A at 298 K.

Discussion

With ΔE_{VI} measured for a series of clusters, we can quantify how a single substitution in the primary coordination sphere affects the valence isomer landscape because, in each cluster, the propensity of the unique ligand to stabilized Fe^{2+} vs $Fe^{2.5+}$ is internally referenced to the other three SIMes-ligated sites. That is, ΔE_{VI} for each cluster can be considered to be referenced to the hypothetical molecule $[(SIMes)_4Fe_4S_4]^+$, which would rigorously have $\Delta E_{VI} = 0$ by virtue of its homoleptic ligand sphere. In this way, $\Delta\Delta E_{VI}$ values can be used to estimate the effect of a single ligand substitution. At the two extremes of the series are ΔE_{VI}(**1-Bn**) = 680 ± 100 cm^{-1} and $\Delta E_{VI}([\mathbf{1\text{-}PhPMe_2}]^+) = -270 \pm 40$ cm^{-1}; we can therefore conclude that a single ligand substitution (in this case, $[Bn]^-$ for $PhPMe_2$) can shift the relative energies of valence isomers by ≥ 10^3 cm^{-1}. The foregoing results thus demonstrate the dramatic impact of the primary coordination sphere on the relative populations of valence isomers in $[Fe_4S_4]^{1+}$ clusters.

Of particular interest are the amino acid side chains known to bind biological $[Fe_4S_4]^{1+}$ clusters. Specifically, comparison of **1-SBn** and [**1-NMI**]$^+$, whose unique ligands ($^-$SBn and NMI) model the sidechains of Cys and His residues, allows for determination of the effects of His ligation on the valence isomer landscape in $[Fe_4S_4]^{1+}$ clusters (Figure 15A). Here, $\Delta\Delta E_{VI} = \Delta E_{VI}$(**1-SBn**) – $\Delta E_{VI}([\mathbf{1\text{-}NMI}]^+) = 210 \pm 60$ cm^{-1}, indicating that a Cys to His mutation is expected to shift ΔE_{VI} by ~200 cm^{-1}. Thus, all things being equal (*i.e.*, ignoring other effects in the active site and differences in the magnetic structures of the two clusters), we would expect replacing one Cys ligand by a His ligand in an $[Fe_4S_4]^{1+}$ to change the probability of the unique Fe being ferrous from 50% to 72% at 298 K (shown schematically in Figure 15B). On this basis, we suggest that part of the effect of non-canonical amino acid (*i.e.*, non-Cys) ligation in Fe–S proteins is to alter the population of valence isomers, with His ligation in particular favoring valence isomers with Fe^{2+} at the His-ligated site.

More generally, we speculate that the composition of the primary sphere, in conjunction with other secondary-sphere effects, may serve to preferentially (de)localize Fe valences in $[Fe_4S_4]^{1+}$ clusters,

facilitating control over electron transfer kinetics and direction by controlling the spatial location of the most reducing Fe ion pair within the cluster. Our work quantitatively and experimentally supports this magnetostructural connection, building on prior experimental findings (*e.g.*, that on *Pf* Fd as discussed above) and theoretical work.[46,124–126] In considering the possibility that non-canonical amino acid ligation of $[Fe_4S_4]$ clusters serves in part to spatially localize Fe valences, we note that in many instances where tight regulation of the direction and timing of electron transfer is thought to be critical, the $[Fe_4S_4]$ clusters that participate in electron transfer processes are site-differentiated.[57,60,61,127,128] Thus, one component of the evolutionary optimization of the primary coordination sphere may be to alter the size, shape, and orientation of holes/electrons in these clusters, with more disperse valence distributions favoring donor/acceptor coupling across a wider number of pathways, a wider range of distances, and lower reorganization energies, and tighter valence distributions favoring more precise donor/acceptor coupling. Indeed, in many instances, mutation of these non-canonical amino acids to give $Cys_4[Fe_4S_4]$ clusters results in complete or partial abolition of enzyme activity, though the effects of valence isomerism are conflated with others; whether the role of the noncanonical amino acid in these systems regulates electron transfer by tuning valence electron localization patterns, altering the magnetic properties of a given valence isomer, or by providing alternate electron tunneling pathways is not always clear, and it is likely that all factors contribute to varying degrees.[49,60,61,129]

Lastly, we place these results in the context of efforts to characterize the dense manifold of low-lying excited states in Fe–S clusters. Although our chosen exchange coupling model is in some ways overly sparse in describing the spin ladder for Fe−S clusters—specifically in adoption of a simplified HDE model[27,29]—the fact that each valence isomer has its own spin ladder substantially increases the density of states for these systems relative to homoleptic systems, particularly in the low energy region. Additionally, we expect that efforts to develop and benchmark quantum chemical methods for computing

the small energy differences between valence isomers will be aided by the experimentally determined ΔE_{VI} values reported herein.

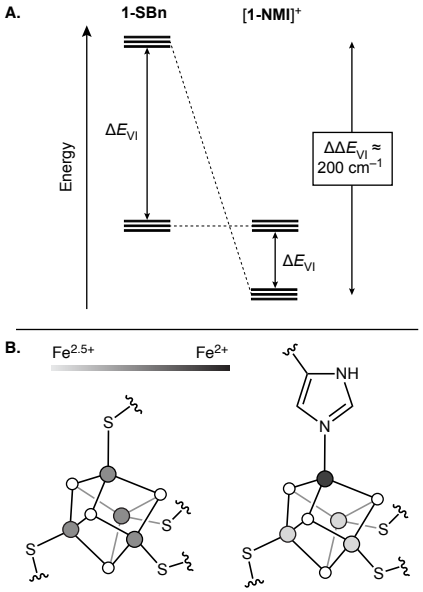

Figure 15. Effect of imidazole/thiolate ligand substitution on the electron distribution in $[Fe_4S_4]^+$ clusters. A) Estimation of $\Delta\Delta E_{VI}$ from **1-SPh** and [**1-NMI**]$^+$. B) Depiction of the effect of His ligation (ignoring all factors beyond the primary coordination sphere).

Conclusion

To summarize, we have described the preparation and characterization of a series of 3:1 site differentiated $[Fe_4S_4]^{1+}$ clusters in which the ligand to the unique Fe site was systematically varied to encompass a wide range of donor/acceptor properties. The magnetic structure of these clusters was quantitatively elucidated through simultaneous fitting of their VT NMR spectra and solution VT magnetic moments. In this manner, we identified for each cluster the ground-state valence isomer, the energy gap to the excited-state valence isomer with a resolution of approximately 0.1 kcal mol^{-1}, and the distribution of valences at ambient temperature (accounting for differences in the spin ladders of each valence isomer). Across the series, the valence isomer offset energies follow trends consistent with the donor/acceptor properties of the unique ligand; the chemically intuitive finding that the more electron-releasing ligands favor the valence isomer in which the unique Fe site is oxidized ($Fe^{2.5+}$) supports the fitting methodology developed herein and the use of a simplified Hamiltonian. We also compared valence isomer offset energies between clusters and learned that single ligand substitutions can alter the energetic landscape of valence isomers by up to 10^3 cm^{-1}, supporting the idea that the non-canonical amino acid ligation can substantially perturb not just the redox properties of the clusters, but also the valence electron distribution as represented by the thermally populated ensemble of states.

Acknowledgements

We thank P. Müller for assistance with XRD experiments. This work was supported by the U.S. Department of Energy, Office of Science, Office of Basic Energy Sciences, Division of Chemical Sciences, Geosciences, and Biosciences under Award #DE-SC0020974 to D.L.M.S. B.A.S. acknowledges fellowships from the National Science Foundation (Graduate Research Fellowship #2141064) and MathWorks. D.S. acknowledges support from the Sloan Foundation and the Camille and Henry Dreyfus Foundation.

Competing interests

The authors declare no competing interests.

Supporting information

Experimental methods, scripts for data analysis, spectroscopic data, and supplementary analysis.

References

(1) Johnson, D. C.; Dean, D. R.; Smith, A. D.; Johnson, M. K. Structure, Function, and Formation of Biological Iron-Sulfur Clusters. *Annu. Rev. Biochem.* **2005**, *74* (1), 247–281.

(2) Johnson, M. K.; Smith, A. D. Iron–Sulfur Proteins. In *Encyclopedia of Inorganic and Bioinorganic Chemistry*; John Wiley & Sons, Ltd, 2011.

(3) DePamphilis, B. V.; Averill, B. A.; Herskovitz, T.; Que, L.; Holm, R. H. Synthetic Analogs of the Active Sites of Iron-Sulfur Proteins. VI. Spectral and Redox Characteristics of the Tetranuclear Clusters $[Fe_4S_4(SR)_4]^{2-}$. *J. Am. Chem. Soc.* **1974**, *96* (13), 4159–4167.

(4) Adman, E.; Watenpaugh, K. D.; Jensen, L. H. NH---S Hydrogen Bonds in Peptococcus Aerogenes Ferredoxin, Clostridium Pasteurianum Rubredoxin, and Chromatium High Potential Iron Protein. *Proc. Natl. Acad. Sci.* **1975**, *72* (12), 4854–4858.

(5) Backes, G.; Mino, Y.; Loehr, T. M.; Meyer, T. E.; Cusanovich, M. A.; Sweeney, W. V.; Adman, E. T.; Sanders-Loehr, J. The Environment of Fe_4S_4 Clusters in Ferredoxins and High-Potential Iron Proteins. New Information from x-Ray Crystallography and Resonance Raman Spectroscopy. *J. Am. Chem. Soc.* **1991**, *113* (6), 2055–2064.

(6) Bertini, I.; Ciurli, S.; Luchinat, C. The Electronic Structure of FeS Centers in Proteins and Models a Contribution to the Understanding of Their Electron Transfer Properties. In *Iron-Sulfur Proteins Perovskites*; Structure and Bonding; Springer: Berlin, Heidelberg, 1995; pp 1–53.

(7) Stephens, P. J.; Jollie, D. R.; Warshel, A. Protein Control of Redox Potentials of Iron−Sulfur Proteins. *Chem. Rev.* **1996**, *96* (7), 2491–2514.

(8) Banci, L.; Bertini, I.; Gori Savellini, G.; Luchinat, C. Individual Reduction Potentials of the Iron Ions in Fe_2S_2 and High-Potential Fe_4S_4 Ferredoxins. *Inorg. Chem.* **1996**, *35* (14), 4248–4253.

(9) Capozzi, F.; Ciurli, S.; Luchinat, C. Coordination Sphere versus Protein Environment as Determinants of Electronic and Functional Properties of Iron-Sulfur Proteins. In *Metal Sites in Proteins and Models Redox Centres*; Hill, H. A. O., Sadler, P. J., Thomson, A. J., Eds.; Structure & Bonding; Springer: Berlin, Heidelberg, 1998; pp 127–160.

(10) Zu, Y.; Couture, M. M.-J.; Kolling, D. R. J.; Crofts, A. R.; Eltis, L. D.; Fee, J. A.; Hirst, J. Reduction Potentials of Rieske Clusters: Importance of the Coupling between Oxidation State and Histidine Protonation State. *Biochemistry* **2003**, *42* (42), 12400–12408.

(11) Niu, S.; Ichiye, T. Insight into Environmental Effects on Bonding and Redox Properties of [4Fe-4S] Clusters in Proteins. *J. Am. Chem. Soc.* **2009**, *131* (16), 5724–5725.

(12) Dey, A.; Jenney, F. E.; Adams, M. W. W.; Babini, E.; Takahashi, Y.; Fukuyama, K.; Hodgson, K. O.; Hedman, B.; Solomon, E. I. Solvent Tuning of Electrochemical Potentials in the Active Sites of HiPIP Versus Ferredoxin. *Science* **2007**, *318* (5855), 1464–1468.

(13) Harris, T. V.; Szilagyi, R. K. Protein Environmental Effects on Iron-Sulfur Clusters: A Set of Rules for Constructing Computational Models for Inner and Outer Coordination Spheres. *J. Comput. Chem.* **2016**, *37* (18), 1681–1696.

(14) Gaughan, S. J. H.; Hirst, J. D.; Croft, A. K.; Jäger, C. M. Effect of Oriented Electric Fields on Biologically Relevant Iron–Sulfur Clusters: Tuning Redox Reactivity for Catalysis. *J. Chem. Inf. Model.* **2022**, *62* (3), 591–601.

(15) Hurley, J. K.; Weber-Main, A. M.; Hodges, A. E.; Stankovich, M. T.; Benning, M. M.; Holden, H. M.; Cheng, H.; Xia, B.; Markley, J. L.; Genzor, C.; Gomez-Moreno, C.; Hafezi, R.; Tollin, G. Iron-Sulfur Cluster Cysteine-to-Serine Mutants of Anabaena [2Fe-2S] Ferredoxin Exhibit Unexpected Redox Properties and Are Competent in Electron Transfer to Ferredoxin:NADP+ Reductase. *Biochemistry* **1997**, *36* (49), 15109–15117.

(16) Achim, C.; Bominaar, E. L.; Meyer, J.; Peterson, J.; Münck, E. Observation and Interpretation of Temperature-Dependent Valence Delocalization in the [2Fe−2S]+ Cluster of a Ferredoxin from Clostridium Pasteurianum. *J. Am. Chem. Soc.* **1999**, *121* (15), 3704–3714.

(17) Ding, X. -Q.; Bill, E.; Trautwein, A. X.; Winkler, H.; Kostikas, A.; Papaefthymiou, V.; Simopoulos, A.; Beardwood, P.; Gibson, J. F. Exchange Interactions, Charge Delocalization, and Spin Relaxation in a Mixed-valence Di-iron Complex Studied by Mössbauer Spectroscopy. *J. Chem. Phys.* **1993**, *99* (9), 6421–6428.
(18) Albers, A.; Demeshko, S.; Dechert, S.; Bill, E.; Bothe, E.; Meyer, F. The Complete Characterization of a Reduced Biomimetic [2Fe-2S] Cluster. *Angew. Chem. Int. Ed.* **2011**, *50* (39), 9191–9194.
(19) Albers, A.; Bayer, T.; Demeshko, S.; Dechert, S.; Meyer, F. A Functional Model for the Rieske Center: Full Characterization of a Biomimetic N-Ligated [2Fe-2S] Cluster in Different Protonation States. *Chem. Eur. J.* **2013**, *19* (31), 10101–10106.
(20) Yao, S.; Meier, F.; Lindenmaier, N.; Rudolph, R.; Blom, B.; Adelhardt, M.; Sutter, J.; Mebs, S.; Haumann, M.; Meyer, K.; Kaupp, M.; Driess, M. Biomimetic [2Fe-2S] Clusters with Extensively Delocalized Mixed-Valence Iron Centers. *Angew. Chem. Int. Ed.* **2015**, *54* (42), 12506–12510.
(21) Papaefthymiou, G. C.; Laskowski, E. J.; Frota-Pessoa, S.; Frankel, R. B.; Holm, R. H. Antiferromagnetic Exchange Interactions in $[Fe_4S_4(SR)_4]^{2-,3-}$ Clusters. *Inorg. Chem.* **1982**, *21* (5), 1723–1728.
(22) Noodleman, L. A Model for the Spin States of High-Potential Iron-Sulfur [Fe4S4]3+ Proteins. *Inorg. Chem.* **1988**, *27* (20), 3677–3679.
(23) Girerd, J.-J.; Papaefthymiou, V.; Surerus, K. K.; Munck, E. Double Exchange in Iron-Sulfur Clusters and a Proposed Spin-Dependent Transfer Mechanism. *Pure Appl. Chem.* **1989**, *61* (5), 805–816.
(24) Borshch, S. A.; Bominaar, E. L.; Blondin, G.; Girerd, J. J. Double Exchange and Vibronic Coupling in Mixed Valence Systems. Origin of the Broken-Symmetry Ground State of $[Fe_3S_4]^0$ Cores in Proteins and Models. *J. Am. Chem. Soc.* **1993**, *115* (12), 5155–5168.
(25) Bominaar, E. L.; Borshch. Serguei A.; Girerd, J.-J. Double-Exchange and Vibronic Coupling in Mixed-Valence Systems. Electronic Structure of $[Fe_4S_4]^{3+}$ Clusters in High-Potential Iron Protein and Related Models. *J. Am. Chem. Soc.* **1994**, *116* (12), 5362–5372.
(26) Bominaar, E. L.; Hu, Z.; Muenck, E.; Girerd, J.-J.; Borshch, S. A. Double Exchange and Vibronic Coupling in Mixed-Valence Systems. Electronic Structure of Exchange-Coupled Siroheme-$[Fe_4S_4]^{2+}$ Chromophore in Oxidized E. Coli Sulfite Reductase. *J. Am. Chem. Soc.* **1995**, *117* (26), 6976–6989.
(27) Sharma, S.; Sivalingam, K.; Neese, F.; Chan, G. K.-L. Low-Energy Spectrum of Iron–Sulfur Clusters Directly from Many-Particle Quantum Mechanics. *Nat. Chem.* **2014**, *6* (10), 927–933.
(28) Benediktsson, B.; Bjornsson, R. QM/MM Study of the Nitrogenase MoFe Protein Resting State: Broken-Symmetry States, Protonation States, and QM Region Convergence in the FeMoco Active Site. *Inorg. Chem.* **2017**, *56* (21), 13417–13429.
(29) Chilkuri, V. G.; DeBeer, S.; Neese, F. Ligand Field Theory and Angular Overlap Model Based Analysis of the Electronic Structure of Homovalent Iron–Sulfur Dimers. *Inorg. Chem.* **2020**, *59* (2), 984–995.
(30) Henthorn, J. T.; Cutsail, G. E.; Weyhermüller, T.; DeBeer, S. Stabilization of Intermediate Spin States in Mixed-Valent Diiron Dichalcogenide Complexes. *Nat. Chem.* **2022**, *14* (3), 328–333.
(31) Beinert, H.; Holm, R. H.; Münck, E. Iron-Sulfur Clusters: Nature's Modular, Multipurpose Structures. *Science* **1997**, *277* (5326), 653–659.
(32) Puschmann, F. F.; Harmer, J.; Stein, D.; Rüegger, H.; de Bruin, B.; Grützmacher, H. Electromeric Rhodium Radical Complexes. *Angew. Chem. Int. Ed.* **2010**, *49* (2), 385–389.
(33) Patra, S. C.; Biswas, M. K.; Maity, A. N.; Ghosh, P. Osazone Anion Radical Complex of Rhodium(III). *Inorg. Chem.* **2011**, *50* (4), 1331–1338.

(34) Cipot-Wechsler, J.; Covelli, D.; Praetorius, J. M.; Hearns, N.; Zenkina, O. V.; Keske, E. C.; Wang, R.; Kennepohl, P.; Crudden, C. M. Synthesis and Characterization of Cationic Rhodium Peroxo Complexes. *Organometallics* **2012**, *31* (21), 7306–7315.
(35) Minkin, V. I.; Starikov, A. G.; Starikova, A. A. Theoretical Modeling of Valence Tautomeric Dinuclear Cobalt Complexes. Adducts of CoII Diketonates with Cyclic Redox-Active Tetraone Ligands. *Dalton Trans.* **2015**, *44* (40), 17819–17828.
(36) Minkin, V. I.; Starikova, A. A.; Starikov, A. G. Quantum Chemical Modeling of Magnetically Bistable Metal Coordination Compounds. Synchronization of Spin Crossover, Valence Tautomerism and Charge Transfer Induced Spin Transition Mechanisms. *Dalton Trans.* **2016**, *45* (30), 12103–12113.
(37) Pokhriyal, D.; Heins, S. P.; Sifri, R. J.; Gentekos, D. T.; Coleman, R. E.; Wolczanski, P. T.; Cundari, T. R.; Fors, B. P.; Lancaster, K. M.; MacMillan, S. N. Reversible C–C Bond Formation, Halide Abstraction, and Electromers in Complexes of Iron Containing Redox-Noninnocent Pyridine-Imine Ligands. *Inorg. Chem.* **2021**, *60* (24), 18662–18673.
(38) Li, X.-X.; Lu, X.; Park, J. W.; Cho, K.-B.; Nam, W. Nonheme Iron Imido Complexes Bearing a Non-Innocent Ligand: A Synthetic Chameleon Species in Oxidation Reactions. *Chem. – Eur. J.* **2021**, *27* (69), 17495–17503.
(39) Müller, B.; Bally, T.; Gerson, F.; de Meijere, A.; von Seebach, M. "Electromers" of the Tetramethyleneethane Radical Cation and Their Nonexistence in the Octamethyl Derivative: Interplay of Experiment and Theory. *J. Am. Chem. Soc.* **2003**, *125* (45), 13776–13783.
(40) Schulte, Y.; Geoghegan, B. L.; Helling, C.; Wölper, C.; Haberhauer, G.; Cutsail, G. E.; Schulz, S. Observation of Discrete Valence Tautomers in Crystalline Cyclopentadienyl Radicals. *J. Am. Chem. Soc.* **2021**, *143* (32), 12658–12664.
(41) Banci, L.; Bertini, I.; Ciurli, S.; Ferretti, S.; Luchinat, C.; Piccioli, M. The Electronic Structure of Iron-Sulfur $[Fe_4S_4]^{3+}$ Clusters in Proteins. An Investigation of the Oxidized High-Potential Iron-Sulfur Protein II from Ectothiorhodospira Vacuolata. *Biochemistry* **1993**, *32* (36), 9387–9397.
(42) Bertini, I.; Ciurli, S.; Dikiy, A.; Luchinat, C. Electronic Structure of the $[Fe_4Se_4]^{3+}$ Clusters in C. Vinosum HiPIP and Ectothiorhodospiza Halophila HiPIP II through NMR and EPR Studies. *J. Am. Chem. Soc.* **1993**, *115* (25), 12020–12028.
(43) Banci, L.; Bertini, I.; Capozzi, F.; Carloni, P.; Ciurli, S.; Luchinat, C.; Piccioli, M. The Iron-Sulfur Cluster in the Oxidized High-Potential Iron Protein from Ectothiorhodospira Halophila. *J. Am. Chem. Soc.* **1993**, *115* (9), 3431–3440.
(44) Bertini, I.; Capozzi, F.; Luchinat, C. Electronic Isomerism in Oxidized High-Potential Iron-Sulfur Proteins Revisited. In *Paramagnetic Resonance of Metallobiomolecules*; ACS Symposium Series; American Chemical Society, 2003; Vol. 858, pp 272–286.
(45) Calzolai, L.; Gorst, C. M.; Bren, K. L.; Zhou, Z.-H.; Adams, M. W. W.; La Mar, G. N. Solution NMR Study of the Electronic Structure and Magnetic Properties of Cluster Ligation Mutants of the Four-Iron Ferredoxin from the Hyperthermophilic Archaeon Pyrococcus Furiosus. *J. Am. Chem. Soc.* **1997**, *119* (40), 9341–9350.
(46) Kubas, A.; Maszota, P. Theoretical Insights into the Unique Ligation of $[Fe_4S_4]$ Iron–Sulfur Clusters. *Eur. J. Inorg. Chem.* **2018**, *2018* (20–21), 2419–2428.
(47) Babini, E.; Bertini, I.; Borsari, M.; Capozzi, F.; Luchinat, C.; Zhang, X.; Moura, G. L. C.; Kurnikov, I. V.; Beratan, D. N.; Ponce, A.; Di Bilio, A. J.; Winkler, J. R.; Gray, H. B. Bond-Mediated Electron Tunneling in Ruthenium-Modified High-Potential Iron−Sulfur Protein. *J. Am. Chem. Soc.* **2000**, *122* (18), 4532–4533.
(48) Calzolai, L.; Zhou, Z. H.; Adams, M. W. W.; La Mar, G. N. Role of Cluster-Ligated Aspartate in Gating Electron Transfer in the Four-Iron Ferredoxin from the Hyperthermophilic Archaeon Pyrococcus Furiosus. *J. Am. Chem. Soc.* **1996**, *118* (10), 2513–2514.

(49) Dementin, S.; Belle, V.; Bertrand, P.; Guigliarelli, B.; Adryanczyk-Perrier, G.; De Lacey, A. L.; Fernandez, V. M.; Rousset, M.; Léger, C. Changing the Ligation of the Distal [4Fe4S] Cluster in NiFe Hydrogenase Impairs Inter- and Intramolecular Electron Transfers. *J. Am. Chem. Soc.* **2006**, *128* (15), 5209–5218.
(50) Dementin, S.; Burlat, B.; Fourmond, V.; Leroux, F.; Liebgott, P.-P.; Abou Hamdan, A.; Léger, C.; Rousset, M.; Guigliarelli, B.; Bertrand, P. Rates of Intra- and Intermolecular Electron Transfers in Hydrogenase Deduced from Steady-State Activity Measurements. *J. Am. Chem. Soc.* **2011**, *133* (26), 10211–10221.
(51) Feng, J.; Shaik, S.; Wang, B. Spin-Regulated Electron Transfer and Exchange-Enhanced Reactivity in Fe_4S_4-Mediated Redox Reaction of the Dph2 Enzyme During the Biosynthesis of Diphthamide. *Angew. Chem. Int. Ed.* **2021**, *60* (37), 20430–20436.
(52) Zhou, S.; Wei, W.-J.; Liao, R.-Z. QM/MM Study of the Mechanism of the Noncanonical S-Cγ Bond Scission in S-Adenosylmethionine Catalyzed by the CmnDph2 Radical Enzyme. *Top. Catal.* **2022**, *65* (1), 517–527.
(53) Wenke, B. B.; Spatzal, T.; Rees, D. C. Site-Specific Oxidation State Assignments of the Iron Atoms in the [4Fe:4S]2+/1+/0 States of the Nitrogenase Fe-Protein. *Angew. Chem. Int. Ed.* **2019**, *58* (12), 3894–3897.
(54) Conover, R. C.; Kowal, A. T.; Fu, W. G.; Park, J. B.; Aono, S.; Adams, M. W.; Johnson, M. K. Spectroscopic Characterization of the Novel Iron-Sulfur Cluster in Pyrococcus Furiosus Ferredoxin. *J. Biol. Chem.* **1990**, *265* (15), 8533–8541.
(55) Telser, J.; Huang, H.; Lee, H.-I.; Adams, M. W. W.; Hoffman, B. M. Site Valencies and Spin Coupling in the 3Fe and 4Fe (S = 1/2) Clusters of Pyrococcus Furiosus Ferredoxin by ^{57}Fe ENDOR. *J. Am. Chem. Soc.* **1998**, *120* (5), 861–870.
(56) Brereton, P. S.; Duderstadt, R. E.; Staples, C. R.; Johnson, M. K.; Adams, M. W. W. Effect of Serinate Ligation at Each of the Iron Sites of the [Fe_4S_4] Cluster of Pyrococcus Furiosus Ferredoxin on the Redox, Spectroscopic, and Biological Properties. *Biochemistry* **1999**, *38* (32), 10594–10605.
(57) Peters, J. W.; Lanzilotta, W. N.; Lemon, B. J.; Seefeldt, L. C. X-Ray Crystal Structure of the Fe-Only Hydrogenase (CpI) from Clostridium Pasteurianum to 1.8 Angstrom Resolution. *Science* **1998**, *282* (5395), 1853–1858.
(58) Bak, D. W.; Elliott, S. J. Alternative FeS Cluster Ligands: Tuning Redox Potentials and Chemistry. *Curr. Opin. Chem. Biol.* **2014**, *19*, 50–58.
(59) Rettberg, L. A.; Wilcoxen, J.; Lee, C. C.; Stiebritz, M. T.; Tanifuji, K.; Britt, R. D.; Hu, Y. Probing the Coordination and Function of Fe_4S_4 Modules in Nitrogenase Assembly Protein NifB. *Nat. Commun.* **2018**, *9* (1), 2824.
(60) E. Lubner, C.; H. Artz, J.; W. Mulder, D.; Oza, A.; J. Ward, R.; Garrett Williams, S.; K. Jones, A.; W. Peters, J.; I. Smalyukh, I.; S. Bharadwaj, V.; W. King, P. A Site-Differentiated [4Fe–4S] Cluster Controls Electron Transfer Reactivity of Clostridium Acetobutylicum [FeFe]-Hydrogenase I. *Chem. Sci.* **2022**, *13* (16), 4581–4588.
(61) Wise, C. E.; Ledinina, A. E.; Lubner, C. E. Site-Differentiated Iron–Sulfur Cluster Ligation Affects Flavin-Based Electron Bifurcation Activity. *Metabolites* **2022**, *12* (9), 823.
(62) Evans, D. F. 400. The Determination of the Paramagnetic Susceptibility of Substances in Solution by Nuclear Magnetic Resonance. *J. Chem. Soc. Resumed* **1959**, No. 0, 2003–2005.
(63) Bain, G. A.; Berry, J. F. Diamagnetic Corrections and Pascal's Constants. *J. Chem. Educ.* **2008**, *85* (4), 532.
(64) Ostfeld, D.; Cohen, I. A. A Cautionary Note on the Use of the Evans Method for Magnetic Moments. *J. Chem. Educ.* **1972**, *49* (12), 829.

(65) Goh, C.; Segal, B. M.; Huang, J.; Long, J. R.; Holm, R. H. Polycubane Clusters: Synthesis of $[Fe_4S_4(PR_3)_4]^{1+,0}$ (R = But, Cy, Pri) and $[Fe_4S_4]^0$ Core Aggregation upon Loss of Phosphine. *J. Am. Chem. Soc.* **1996**, *118* (47), 11844–11853.

(66) Poe, M.; Phillips, W. D.; McDonald, C. C.; Lovenberg, W. Proton Magnetic Resonance Study of Ferredoxin from Clostridium Pasteurianum*. *Proc. Natl. Acad. Sci.* **1970**, *65* (4), 797–804.

(67) Phillips, W. D.; Poe, M.; McDonald, C. C.; Bartsch, R. G. Proton Magnetic Resonance Studies of Chromatium High-Potential Iron Protein. *Proc. Natl. Acad. Sci.* **1970**, *67* (2), 682–687.

(68) Holm, R. H.; Phillips, W. D.; Averill, B. A.; Mayerle, J. J.; Herskovitz, T. Synthetic Analogs of the Active Sites of Iron-Sulfur Proteins. V. Proton Resonance Properties of the Tetranuclear Clusters [Tetra-.Mu.-Sulfido-Tetrakis(Alkyl or Aryl Thiolato)Tetraferrate](2-). *J. Am. Chem. Soc.* **1974**, *96* (7), 2109–2117.

(69) Reynolds, J. G.; Laskowski, E. J.; Holm, R. H. Proton Magnetic Resonance Properties of the Tetranuclear Clusters $[Fe_4S_4(SR)_4]^{3-}$, Analogs of the 4-Fe Sites of Reduced Ferredoxins. *J. Am. Chem. Soc.* **1978**, *100* (17), 5315–5322.

(70) Busse, S. C.; La Mar, G. N.; Yu, L. P.; Howard, J. B.; Smith, E. T.; Zhou, Z. H.; Adams, M. W. W. Proton NMR Investigation of the Oxidized Three-Iron Clusters in the Ferredoxins from the Hyperthermophilic Archae Pyrococcus Furiosus and Thermococcus Litoralis. *Biochemistry* **1992**, *31* (47), 11952–11962.

(71) Macedo, A. L.; Moura, I.; Moura, J. J. G.; Le Gall, J.; Huynh Boi Hanh. Temperature-Dependent Proton NMR Investigation of the Electronic Structure of the Trinuclear Iron Cluster of the Oxidized Desulfovibrio Gigas Ferredoxin II. *Inorg. Chem.* **1993**, *32* (7), 1101–1105.

(72) Banci, L.; Bertini, I.; Eltis, L. D.; Felli, I. C.; Kastrau, D. H. W.; Luchinat, C.; Piccioli, M.; Pierattelli, R.; Smith, M. The Three-Dimensional Structure in Solution of the Paramagnetic High-Potential Iron-Sulfur Protein I from Ectothiorhodospira Halophila through Nuclear Magnetic Resonance. *Eur. J. Biochem.* **1994**, *225* (2), 715–725.

(73) Bertini, I.; Donaire, A.; Feinberg, B. A.; Luchinat, C.; Picciolp, M.; Yuan, H. Solution Structure of the Oxidized 2[4Fe-4S] Ferredoxin from Clostridium Pasteurianum. *Eur. J. Biochem.* **1995**, *232* (1), 192–205.

(74) Bertini, I.; Luchinat, C.; Rosato, A. NMR Spectra of Iron-Sulfur Proteins. In *Advances in Inorganic Chemistry*; Sykes, A. G., Ed.; Academic Press, 1999; Vol. 47, pp 251–282.

(75) Camponeschi, F.; Gallo, A.; Piccioli, M.; Banci, L. The Long-Standing Relationship between Paramagnetic NMR and Iron–Sulfur Proteins: The MitoNEET Example. An Old Method for New Stories or the Other Way Around? *Magn. Reson.* **2021**, *2* (1), 203–221.

(76) Bertini, I.; Luchinat, C.; Parigi, G.; Ravera, E. Chapter 2 - The Hyperfine Shift. In *NMR of Paramagnetic Molecules (Second Edition)*; Bertini, I., Luchinat, C., Parigi, G., Ravera, E., Eds.; Elsevier: Boston, 2017; pp 25–60.

(77) Jordanov, J.; Roth, E. K. H.; Fries, P. H.; Noodleman, L. Magnetic Studies of the High-Potential Protein Model $[Fe_4S_4(S\text{-}2,4,6\text{-}(Iso\text{-}Pr)_3C_6H_2)_4]^-$ in the $[Fe_4S_4]^{3+}$ Oxidized State. *Inorg. Chem.* **1990**, *29* (21), 4288–4292.

(78) Noodleman, L. Exchange Coupling and Resonance Delocalization in Reduced Iron-Sulfur $[Fe_4S_4]^+$ and Iron-Selenium $[Fe_4Se_4]^+$ Clusters. 1. Basic Theory of Spin-State Energies and EPR and Hyperfine Properties. *Inorg. Chem.* **1991**, *30* (2), 246–256.

(79) Noodleman, L. Exchange Coupling and Resonance Delocalization in Reduced Iron-Sulfur $[Fe_4S_4]^+$ and Iron-Selenium $[Fe_4Se_4]^+$ Clusters. 2. A Generalized Nonlinear Model for Spin-State Energies and EPR and Hyperfine Properties. *Inorg. Chem.* **1991**, *30* (2), 256–264.

(80) Kappl, R.; Ciurli, S.; Luchinat, C.; Hüttermann, J. Probing Structural and Electronic Properties of the Oxidized $[Fe_4S_4]^{3+}$ Cluster of Ectothiorhodospira Halophila Iso-II High-Potential Iron−Sulfur Protein by ENDOR Spectroscopy. *J. Am. Chem. Soc.* **1999**, *121* (9), 1925–1935.

(81) Banci, L.; Bertini, I.; Briganti, F.; Luchinat, C.; Scozzafava, A.; Oliver, M. V. Proton NMR Spectra of Oxidized High-Potential Iron-Sulfur Protein (HiPIP) from Rhodocyclus Gelatinosus. A Model for Oxidized HiPIPs. *Inorg. Chem.* **1991**, *30* (24), 4517–4524.

(82) Laskowski, E. J.; Frankel, R. B.; Gillum, W. O.; Papaefthymiou, G. C.; Renaud, J.; Ibers, J. A.; Holm, R. H. Synthetic Analogs of the 4-Fe Active Sites of Reduced Ferredoxins. Electronic Properties of the Tetranuclear Trianions $[Fe_4S_4(SR)_4]^{3-}$ and the Structure of $[(C_2H_5)_3(CH_3)N]_3[Fe_4S_4(SC_6H_5)_4]$. *J. Am. Chem. Soc.* **1978**, *100* (17), 5322–5337.

(83) Bertini, I.; Briganti, F.; Luchinat, C.; Messori, L.; Monnanni, R.; Scozzafava, A.; Vallini, G. 1H-NMR Studies on Partially and Fully Reduced 2(4Fe-4S) Ferredoxin from Clostridium Pasteurianum. *Eur. J. Biochem.* **1992**, *204* (2), 831–839.

(84) Crozet, M.; Chaussade, M.; Bardet, M.; Emsley, L.; Lamotte, B.; Mouesca, J.-M. Carbon-13 Solid-State NMR Studies on Synthetic Model Compounds of [4Fe−4S] Clusters in the 2+ State. *J. Phys. Chem. A* **2000**, *104* (44), 9990–10000.

(85) Noodleman, L.; Peng, C. Y.; Case, D. A.; Mouesca, J.-M. Orbital Interactions, Electron Delocalization and Spin Coupling in Iron-Sulfur Clusters. *Coord. Chem. Rev.* **1995**, *144*, 199–244.

(86) Ciurli, S.; Carrie, M.; Weigel, J. A.; Carney, M. J.; Stack, T. D. P.; Papaefthymiou, G. C.; Holm, R. H. Subsite-Differentiated Analogs of Native Iron Sulfide [4Fe-4S]2+ Clusters: Preparation of Clusters with Five- and Six-Coordinate Subsites and Modulation of Redox Potentials and Charge Distributions. *J. Am. Chem. Soc.* **1990**, *112* (7), 2654–2664.

(87) Noodleman, L.; Case, D. A.; Mouesca, J.-M.; Lamotte, B. Valence Electron Delocalization in Polynuclear Iron-Sulfur Clusters. *JBIC J. Biol. Inorg. Chem.* **1996**, *1* (2), 177–182.

(88) Ye, M.; Thompson, N. B.; Brown, A. C.; Suess, D. L. M. A Synthetic Model of Enzymatic $[Fe_4S_4]$–Alkyl Intermediates. *J. Am. Chem. Soc.* **2019**, *141* (34), 13330–13335.

(89) Brown, A. C.; Suess, D. L. M. Controlling Substrate Binding to Fe_4S_4 Clusters through Remote Steric Effects. *Inorg. Chem.* **2019**, *58* (8), 5273–5280.

(90) Brown, A. C.; Suess, D. L. M. Reversible Formation of Alkyl Radicals at $[Fe_4S_4]$ Clusters and Its Implications for Selectivity in Radical SAM Enzymes. *J. Am. Chem. Soc.* **2020**, *142* (33), 14240–14248.

(91) Sridharan, A.; Brown, A. C.; Suess, D. L. M. A Terminal Imido Complex of an Iron–Sulfur Cluster. *Angew. Chem. Int. Ed.* **2021**, *60* (23), 12802–12806.

(92) Brown, A. C.; Suess, D. L. M. Valence Localization in Alkyne and Alkene Adducts of Synthetic $[Fe_4S_4]^+$ Clusters. *Inorg. Chem.* **2022**.

(93) Kim, Y.; Sridharan, A.; Suess, D. L. M. The Elusive Mononitrosylated $[Fe_4S_4]$ Cluster in Three Redox States. *Angew. Chem. Int. Ed.* **2022**, *61* (47), e202213032.

(94) Arduengo, A. J. III.; Goerlich, J. R.; Marshall, W. J. A Stable Diaminocarbene. *J. Am. Chem. Soc.* **1995**, *117* (44), 11027–11028.

(95) Peters, J. C.; Johnson, A. R.; Odom, A. L.; Wanandi, P. W.; Davis, W. M.; Cummins, C. C. Assembly of Molybdenum/Titanium μ-Oxo Complexes via Radical Alkoxide C−O Cleavage. *J. Am. Chem. Soc.* **1996**, *118* (42), 10175–10188.

(96) Brown, A. C.; Thompson, N. B.; Suess, D. L. M. Evidence for Low-Valent Electronic Configurations in Iron–Sulfur Clusters. *J. Am. Chem. Soc.* **2022**, *144* (20), 9066–9073.

(97) Phillips, W. D.; McDonald, C. C.; Stombaugh, N. A.; Orme-Johnson, W. H. Proton Magnetic Resonance and Magnetic Susceptibility Characterization of Ferredoxin I from Bacillus Polymyxa. *Proc. Natl. Acad. Sci.* **1974**, *71* (1), 140–143.

(98) Moura, JoséJ. G.; Xavier, A. V.; Bruschi, M.; Gall, J. L. NMR Characterization of Three Forms of Ferredoxin from Desulphovibrio Gigas, a Sulphate Reducer. *Biochim. Biophys. Acta BBA - Bioenerg.* **1977**, *459* (2), 278–289.

(99) Bertini, I.; Capozzi, F.; Luchinat, C.; Piccioli, M.; Vila, A. J. The Iron-Sulfur Cluster (Fe_4S_4) Centers in Ferredoxins Studied through Proton and Carbon Hyperfine Coupling. Sequence-Specific Assignments of Cysteines in Ferredoxins from Clostridium Acidi Urici and Clostridium Pasteurianum. *J. Am. Chem. Soc.* **1994**, *116* (2), 651–660.

(100) Ollerenshaw, T. J.; Bristow, S.; Anand, B. N.; Garner, C. D. Carbon-13 Nuclear Magnetic Resonance Studies of Synthetic $[Fe_4S_4(SR)_4]^{2-}$ Iron Sulphur Clusters. *J. Chem. Soc. Dalton Trans.* **1986**, No. 9, 2013–2015.

(101) Barbaro, P.; Bencini, A.; Bertini, I.; Briganti, F.; Midollini, S. The Tetranuclear Trianion $[Fe_4Te_4(SC_6H_5)_4]^{3-}$: Crystal and Molecular Structure and Magnetic Properties. *J. Am. Chem. Soc.* **1990**, *112* (20), 7238–7246.

(102) Sanakis, Y.; Yoo, S. J.; Osterloh, F.; Holm, R. H.; Münck, E. Determination of Antiferromagnetic Exchange Coupling in the Tetrahedral Thiolate-Bridged Diferrous Complex $[Fe_2(SEt)_6]^{2-}$. *Inorg. Chem.* **2002**, *41* (26), 7081–7085.

(103) Belinskii, M.; Bertini, I.; Galas, O.; Luchinat, C. The Electronic Structure of the $Fe_4S_4^{+3}$ Cluster in Proteins: The Importance of Double Exchange Parameter. *Z. Für Naturforschung A* **1995**, *50* (1), 75–80.

(104) Blondin, G.; Girerd, J.-J. Value of the β Transfer Integral in Fe-S Clusters. *JBIC J. Biol. Inorg. Chem.* **1996**, *1* (2), 170–172.

(105) Exchange versus Double Exchange in Polymetallic Fe-S Systems. *JBIC J. Biol. Inorg. Chem.* **1996**, *1* (2), 169–169.

(106) Lawson Daku, L. M.; Pécaut, J.; Lenormand-Foucaut, A.; Vieux-Melchior, B.; Iveson, P.; Jordanov, J. Investigation of the Reduced High-Potential Iron−Sulfur Protein from Chromatium Vinosum and Relevant Model Compounds: A Unified Picture of the Electronic Structure of $[Fe_4S_4]^{2+}$ Systems through Magnetic and Optical Studies. *Inorg. Chem.* **2003**, *42* (21), 6824–6850.

(107) Priem, A. H.; Klaassen, A. A. K.; Reijerse, E. J.; Meyer, T. E.; Luchinat, C.; Capozzi, F.; Dunham, W. R.; Hagen, W. R. EPR Analysis of Multiple Forms of [4Fe–4S]3+ Clusters in HiPIPs. *JBIC J. Biol. Inorg. Chem.* **2005**, *10* (4), 417–424.

(108) Gloux, J.; Gloux, P.; Lamotte, B.; Mouesca, J.-M.; Rius, G. The Different $[Fe_4S_4]^{3+}$ and $[Fe_4S_4]^{+}$ Species Created by .Gamma. Irradiation in Single Crystals of the $(Et_4N)_2[Fe_4S_4(SBenz)_4]$ Model Compound: Their EPR Description and Their Biological Significance. *J. Am. Chem. Soc.* **1994**, *116* (5), 1953–1961.

(109) Le Pape, L.; Lamotte, B.; Mouesca, J.-M.; Rius, G. Paramagnetic States of Four Iron−Four Sulfur Clusters. 1. EPR Single-Crystal Study of 3+ and 1+ Clusters of an Asymmetrical Model Compound and General Model for the Interpretation of the g-Tensors of These Two Redox States. *J. Am. Chem. Soc.* **1997**, *119* (41), 9757–9770.

(110) Le Pape, L.; Lamotte, B.; Mouesca, J.-M.; Rius, G. Paramagnetic States of Four Iron−Four Sulfur Clusters. 2. Proton ENDOR Study of a 1+ State in an Asymmetrical Cluster. *J. Am. Chem. Soc.* **1997**, *119* (41), 9771–9781.

(111) Moriaud, F.; Gambarelli, S.; Lamotte, B.; Mouesca, J.-M. Detailed Proton Q-Band ENDOR Study of the Electron Spin Population Distribution in the Reduced [4Fe-4S]1+ State. *J. Phys. Chem. B* **2001**, *105* (39), 9631–9642.

(112) Antanaitis, B. C.; Moss, T. H. Magnetic Studies of the Four-Iron High-Potential, Non-Heme Protein from Chromatium Vinosum. *Biochim. Biophys. Acta BBA - Protein Struct.* **1975**, *405* (2), 262–279.

(113) McSkimming, A.; Sridharan, A.; Thompson, N. B.; Müller, P.; Suess, D. L. M. An $[Fe_4S_4]^{3+}$–Alkyl Cluster Stabilized by an Expanded Scorpionate Ligand. *J. Am. Chem. Soc.* **2020**, *142* (33), 14314–14323.

(114) Cowan, J. A.; Sola, M. Proton NMR Studies of Oxidized High-Potential Iron Protein from Chromatium Vinosum. Nuclear Overhauser Effect Measurements. *Biochemistry* **1990**, *29* (23), 5633–5637.
(115) Busse, S. C.; La Mar, G. N.; Howard, J. B. Two-Dimensional NMR Investigation of Iron-Sulfur Cluster Electronic and Molecular Structure of Oxidized Clostridium Pasteurianum Ferredoxin. Interpretability of Contact Shifts in Terms of Cysteine Orientation. *J. Biol. Chem.* **1991**, *266* (35), 23714–23723.
(116) Mouesca, J.-M.; Rius, G.; Lamotte, B. Single-Crystal Proton ENDOR Studies of the $[Fe_4S_4]^{3+}$ Cluster: Determination of the Spin Population Distribution and Proposal of a Model to Interpret the ^1H NMR Paramagnetic Shifts in High-Potential Ferredoxins. *J. Am. Chem. Soc.* **1993**, *115* (11), 4714–4731.
(117) Bordwell, F. G. Equilibrium Acidities in Dimethyl Sulfoxide Solution. *Acc. Chem. Res.* **1988**, *21* (12), 456–463.
(118) Haav, K.; Saame, J.; Kütt, A.; Leito, I. Basicity of Phosphanes and Diphosphanes in Acetonitrile. *Eur. J. Org. Chem.* **2012**, *2012* (11), 2167–2172.
(119) Yu, H.-Z.; Yang, Y.-M.; Zhang, L.; Dang, Z.-M.; Hu, G.-H. Quantum-Chemical Predictions of PKa's of Thiols in DMSO. *J. Phys. Chem. A* **2014**, *118* (3), 606–622.
(120) Thapa, B.; Schlegel, H. B. Theoretical Calculation of PKa's of Selenols in Aqueous Solution Using an Implicit Solvation Model and Explicit Water Molecules. *J. Phys. Chem. A* **2016**, *120* (44), 8916–8922.
(121) Tshepelevitsh, S.; Kütt, A.; Lõkov, M.; Kaljurand, I.; Saame, J.; Heering, A.; Plieger, P. G.; Vianello, R.; Leito, I. On the Basicity of Organic Bases in Different Media. *Eur. J. Org. Chem.* **2019**, *2019* (40), 6735–6748.
(122) Schenck, G.; Baj, K.; Iggo, J. A.; Wallace, M. Efficient PKa Determination in a Nonaqueous Solvent Using Chemical Shift Imaging. *Anal. Chem.* **2022**, *94* (23), 8115–8119.
(123) Bonasia, P. J.; Christou, V.; Arnold, J. Alkyl-, Silyl-, and Germyl-Substituted Thiolate, Selenolate, and Tellurolate Derivatives and Interconversion of Silyl Species by Chalcogen Metathesis. *J. Am. Chem. Soc.* **1993**, *115* (15), 6777–6781.
(124) Bominaar, E. L.; Achim, C.; Borshch, S. A.; Girerd, J.-J.; Münck, E. Analysis of Exchange Interaction and Electron Delocalization as Intramolecular Determinants of Intermolecular Electron-Transfer Kinetics. *Inorg. Chem.* **1997**, *36* (17), 3689–3701.
(125) Bominaar, E. L.; Achim, C.; Borshch, S. A. Theory for Electron Transfer from a Mixed-Valence Dimer with Paramagnetic Sites to a Mononuclear Acceptor. *J. Chem. Phys.* **1999**, *110* (23), 11411–11422.
(126) Kubas, A. How the Donor/Acceptor Spin States Affect the Electronic Couplings in Molecular Charge-Transfer Processes? *J. Chem. Theory Comput.* **2021**, *17* (5), 2917–2927.
(127) Volbeda, A.; Charon, M.-H.; Piras, C.; Hatchikian, E. C.; Frey, M.; Fontecilla-Camps, J. C. Crystal Structure of the Nickel–Iron Hydrogenase from Desulfovibrio Gigas. *Nature* **1995**, *373* (6515), 580–587.
(128) Muraki, N.; Nomata, J.; Ebata, K.; Mizoguchi, T.; Shiba, T.; Tamiaki, H.; Kurisu, G.; Fujita, Y. X-Ray Crystal Structure of the Light-Independent Protochlorophyllide Reductase. *Nature* **2010**, *465* (7294), 110–114.
(129) Hayashi, T.; Stuchebrukhov, A. A. Electron Tunneling in Respiratory Complex I. *Proc. Natl. Acad. Sci.* **2010**, *107* (45), 19157–19162.